

PLUG-AND-PLAY IMAGE RESTORATION WITH FLOW MATCHING: A CONTINUOUS VIEWPOINT

FAN JIA, YUHAO HUANG, SHIH-HSIN WANG, CRISTINA GARCIA-CARDONA, ANDREA L. BERTOZZI,
AND BAO WANG

ABSTRACT. Flow matching-based generative models have been integrated into the plug-and-play (PnP) image restoration framework, yielding the PnP-Flow model that has achieved remarkable empirical success. However, its theoretical understanding remains limited. In this paper, we derive a continuous-limit stochastic differential equation (SDE) surrogate for PnP-Flow. This continuous viewpoint provides two key insights: (1) it enables rigorous error quantification, guiding improved step scheduling and Lipschitz regularization of the neural vector field; (2) it motivates an extrapolation-based acceleration strategy for off-the-shelf PnP-Flow models. Extensive experiments on image denoising, deblurring, super-resolution, and inpainting demonstrate that our SDE-informed enhancements significantly outperform baseline PnP-Flow and competing state-of-the-art methods across standard metrics.

1. INTRODUCTION

Image restoration seeks to reconstruct high-quality images suffering from degradations, such as noisy [6, 12, 21, 32], blurry [49, 50, 35], low-resolution [15, 13], enhancement [44, 28, 20], and foreground occlusions [3, 48, 23]. The relationship between an unknown high-quality image $\mathbf{x} \in \mathbb{R}^n$ and a degraded observation $\boldsymbol{\omega} \in \mathbb{R}^m$ can be modeled as

$$\boldsymbol{\omega} = \mathcal{A}\mathbf{x} + \boldsymbol{\nu},$$

where $\mathcal{A} : \mathbb{R}^n \rightarrow \mathbb{R}^m$ is a degradation operator that can be linear or nonlinear, and $\boldsymbol{\nu}$ represents the underlying additive noise. Traditional approaches often formulate this as an optimization problem, minimizing a well-designed objective function—that balances a data fidelity term $f(\cdot)$ and a regularization term $g(\cdot)$ reflecting image priors—as follows:

$$\mathbf{x}^* = \arg \min_{\mathbf{x}} f(\mathbf{x}) + g(\mathbf{x}),$$

where $f(\mathbf{x})$ is often defined to be $\frac{1}{2}\|\mathcal{A}\mathbf{x} - \boldsymbol{\omega}\|^2$ when $\boldsymbol{\nu}$ is a zero-mean Gaussian noise.

Crafting an effective regularizer for complex priors is challenging, and the plug-and-play (PnP) framework [41] addresses this by replacing the explicit regularizer $g(\mathbf{z})$ with an implicit prior—often a pre-trained neural network (NN) denoiser. PnP combines the flexibility of optimization methods with the expressivity of NN, achieving state-of-the-art (SOTA) performance across various tasks. Leveraging their impressive performance in image generation, generative models have been adopted within the PnP framework (cf. [43, 38, 52]). A noticeable generative model is based on flow matching (FM) [25], which learns a vector field with associated probability density path interpolating between a prior and the data distributions, offering computational efficiency through deterministic ordinary differential equation (ODE) flows [7]. Integrating FM into PnP, termed PnP-Flow [29], has shown promising empirical results.

While PnP methods with learned implicit priors (e.g., NNs or generative models) often outperform traditional approaches empirically, their theoretical analysis is complex. Implicit regularizers may

2020 *Mathematics Subject Classification.* 68T07, 68U10, 94A08, 65K10.

Key words and phrases. image restoration, generative models, flow matching, plug-and-play methods, stochastic differential equations.

not satisfy assumptions required by classical optimization tools, limiting insights into convergence or error bounds. To address this issue, by assuming NNs possess specific properties, such as being Lipschitz differentiable or convex, provably convergent PnP methods have been developed with rigorous convergence analysis [40, 36, 11]. However, convergence and error bounds for PnP with generative models still remain largely unaddressed.

In this paper, we propose a continuous perspective on PnP-Flow by modeling it with a stochastic differential equation (SDE). The SDE formulation is not merely a mathematical reformulation—it provides fundamental insights that bridge the theoretical gap in PnP frameworks and enables principled design of guidance algorithms as well as training loss functions across generative models. This approach introduces novel analytical tools to characterize key parameters governing convergence rates and error bounds within the PnP framework.

1.1. Our Contributions. We aim to enhance our understanding of PnP-Flow and improve its performance and efficiency in a principled manner. Our key contributions are:

- **Continuous Limit Derivation:** We show that the continuous-in-time (iteration) limit of PnP-Flow is an SDE; see Section 3.
- **Error Quantification:** Using the SDE surrogate model, we bound the image restoration error for PnP-Flow, highlighting the roles of the Lipschitz constant of the NN-parameterized vector field and step scheduling in error reduction; see Section 4.
- **Theoretically-Principled Improvement:** We propose 1) a new step scheduling for PnP-Flow, 2) an efficient Lipschitz regularization based on Hutchinson’s method [18], and 3) an extrapolated iteration to enhance efficiency without retraining; see Section 5.
- **Empirical Validation:** We validate the advantages of our improved PnP-Flow using various benchmark tasks; see Section 6.

1.2. Additional Related Works. Using generative models as PnP denoisers within an iterative framework is an emerging research area. As one of the earliest works in this direction, [5] demonstrates that generative models could act as powerful priors for compressed sensing. Subsequent developments extend this idea to generative adversarial network (GAN)-based approaches [37], score-based generative methods [22], and more recently, diffusion models (DMs) tailored for inverse problem-solving [10, 9]. Recent advances further propose PnP frameworks that alternate between likelihood and DM sampling for general inverse problems [43, 45].

1.3. Organization. We structure this paper as follows: We review FM and PnP-Flow in Section 2. We derive the SDE-limit of PnP-Flow in Section 3. We analyze the PnP-Flow error and present improved PnP-Flow in Sections 4 and 5, respectively. We validate the efficacy and efficiency of the improved PnP-Flow, together with ablation studies, in Section 6. Technical proofs and additional experimental details are provided in the appendix.

2. PRELIMINARIES

2.1. Flow Matching with Straight-Line Paths. FM (cf. [25, 1, 26]) learns a vector field that induces a probability density path interpolating between a prior distribution q (e.g., the standard Gaussian $\mathcal{N}(\mathbf{0}, \mathbf{I})$) and the data distribution p . Mathematically, for a given vector field $\mathbf{u}_t : [0, 1] \times \mathbb{R}^d \rightarrow \mathbb{R}^d$, it defines a flow $\phi_t : [0, 1] \times \mathbb{R}^n \rightarrow \mathbb{R}^n$ via the following ODE:

$$(1) \quad \frac{d}{dt} \phi_t(\mathbf{x}) = \mathbf{u}_t(\phi_t(\mathbf{x})), \quad \phi_0(\mathbf{x}) = \mathbf{x}_0.$$

The flow ϕ_t interpolates between the noise sample $\phi_0(\mathbf{x}) = \mathbf{x}_0 \sim q$ and the data sample $\phi_1(\mathbf{x}) = \mathbf{x}_1 \sim p$. Moreover, ϕ_t induces a probability path, defined as $p_t(\mathbf{x}) = p_0(\phi_t^{-1}(\mathbf{x})) \det[\frac{\partial \phi_t^{-1}(\mathbf{x})}{\partial \mathbf{x}}]$, $\forall \mathbf{x} \in p_0 = q$, interpolates between the prior ($p_0 = q$) and data ($p_1 = p$) distributions. In practice, the vector field \mathbf{u}_t is unavailable, which is only defined—in its conditional form $\mathbf{u}_t(\cdot | \mathbf{x}_1)$ —for each training data

$\mathbf{x}_1 \sim p$. FM regresses a neural network $\tilde{\mathbf{u}}_t(\cdot, \theta)$ —with θ being learnable parameters—against $\mathbf{u}_t(\cdot|\mathbf{x}_1)$ for each training data, resulting in an unbiased estimate for the unconditional vector field \mathbf{u}_t [25]; this process is named conditional flow matching (cf. [25]). The learned vector field $\tilde{\mathbf{u}}_t(\cdot, \theta)$ drives any noise sample to a generated realistic data.

In [26, 29], the authors construct a straight-line path for FM as follows: for any $\mathbf{x}_1 \sim p$, we can define a conditional flow $\phi_t(\mathbf{x}|\mathbf{x}_1) = (1-t)\mathbf{x} + t\mathbf{x}_1$. The corresponding conditional vector field is $\mathbf{u}_t(\phi_t(\mathbf{x})|\mathbf{x}_1) = \mathbf{x}_1 - \mathbf{x}$. While other path formulations for flow matching exist, straight-line paths give a concise form of $\phi_t(\mathbf{x}|\mathbf{x}_1)$ and simplify training and implementation. For simplicity, we denote $\mathbf{u}_t(\mathbf{x}_t)$ as in [29], where it represents $\mathbf{u}_t(\mathbf{x}_t|\mathbf{x}_1)$. The definition and implementation of the optimal transport (OT) flow and \mathbf{u}_t in our paper are consistent with those in [29].

2.2. PnP-Flow for Image Restoration. Given a minimization problem

$$(2) \quad \min_{\mathbf{x}} f(\mathbf{x}) + g(\mathbf{x}),$$

the proximal gradient method solves eq. (2) by the following iteration:

$$(3) \quad \begin{cases} \mathbf{z}_{k+1} = \mathbf{x}_k - \gamma_k \nabla f(\mathbf{x}_k), \\ \mathbf{x}_{k+1} = \text{prox}_{\gamma_k g}(\mathbf{z}_{k+1}), \end{cases}$$

where the proximal operator is defined as:

$$\text{prox}_{\gamma_k g}(\mathbf{z}) = \arg \min_{\mathbf{x}} g(\mathbf{x}) + \frac{1}{2\gamma_k} \|\mathbf{x} - \mathbf{z}\|_2^2.$$

As PnP methods generally replace the proximal operator with an off-the-shelf denoiser, PnP-Flow [29] replaces the proximal operator in eq. (3) by an FM process, resulting in

$$(4) \quad \begin{cases} \mathbf{z}_k = \mathbf{x}_k - \gamma_k \nabla f(\mathbf{x}_k), \\ \mathbf{y}_k = (1-l_k)\boldsymbol{\xi} + l_k \mathbf{z}_k, \quad \boldsymbol{\xi} \sim \mathcal{N}(0, \mathbf{I}), \\ \mathbf{x}_{k+1} = D_{l_k}(\mathbf{y}_k), \end{cases}$$

where l_k increases with $l_0 = 0$ and $\lim_{k \rightarrow \infty} l_k = 1$, and $D_{l_k} := \text{Id} + (1-l_k)\mathbf{u}_{l_k}$ with \mathbf{u}_{l_k} being the vector field of the FM model. The following remark provides rationale for eq. (4).

Remark 1. *Instead of solving eq. (1), [29] suggests that the operator $D_t(\mathbf{x}_t) = [\text{Id} + (1-t)\mathbf{u}_t] \circ \mathbf{x}_t$ with Id being the identity, can be interpreted as the best approximation of \mathbf{x}_1 given the knowledge of \mathbf{x}_t . Moreover, the second step in eq. (4) projects \mathbf{z}_k to the straight-line path.*

The convergence of the iteration process in eq. (4) is guaranteed as follows:

Proposition 2.2.1. [29, Proposition 4] *Assume that $f: \mathbb{R}^n \rightarrow \mathbb{R}$ is continuously differentiable and the learned vector field $\tilde{\mathbf{u}}_t(\cdot, \theta)$ is continuous. Let $\{l_k\}_{k \in \mathbb{N}}$ satisfy $\sum_{k=0}^{\infty} (1-l_k) < +\infty$ and $\gamma_k := 1-l_k$. If $\{\mathbf{x}_k\}_{k \in \mathbb{N}}$ obtained by eq. (4) with $\tilde{\mathbf{u}}_t(\cdot, \theta)$ is bounded, then it converges.*

3. THE CONTINUOUS LIMIT OF PNP-FLOW

As the first contribution, we derive an SDE model for eq. (4). Plugging $D_{l_k} := \text{Id} + (1-l_k)\mathbf{u}_{l_k}$ into the last equation of eq. (4), we have

$$(5) \quad \begin{aligned} \mathbf{x}_{k+1} &= [\text{Id} + (1-l_k)\mathbf{u}_{l_k}] \circ (\mathbf{y}_k) \\ &= (1-l_k)\boldsymbol{\xi} + l_k \mathbf{z}_k + (1-l_k)\mathbf{u}_{l_k}(\mathbf{y}_k) \\ &= (1-l_k)\boldsymbol{\xi} + l_k(\mathbf{x}_k - \gamma_k \nabla f(\mathbf{x}_k)) + (1-l_k)\mathbf{u}_{l_k}(\mathbf{y}_k). \end{aligned}$$

Applying Taylor expansion to \mathbf{u}_{l_k} with respect to \mathbf{y}_k at point \mathbf{x}_k gives

$$(6) \quad \mathbf{u}_{l_k}(\mathbf{y}_k) = \mathbf{u}_{l_k}(\mathbf{x}_k) + (\mathbf{y}_k - \mathbf{x}_k) \nabla \mathbf{u}_{l_k}(\mathbf{x}_k) + o(\mathbf{y}_k - \mathbf{x}_k).$$

Moreover, by the first two equations in eq. (4), we have

$$\begin{aligned}\mathbf{y}_k - \mathbf{x}_k &= (1 - l_k)\boldsymbol{\xi} + l_k \mathbf{z}_k - \mathbf{x}_k \\ &= (1 - l_k)(\boldsymbol{\xi} - \mathbf{x}_k) - l_k \gamma_k \nabla f(\mathbf{x}_k),\end{aligned}$$

let $\beta_k = \frac{l_k \gamma_k}{1 - l_k}$, we have

$$(7) \quad \mathbf{y}_k - \mathbf{x}_k = (1 - l_k)(\boldsymbol{\xi} - \mathbf{x}_k - \beta_k \nabla f(\mathbf{x}_k)).$$

Combining eqs. (5) to (7), we have

$$(8) \quad \begin{aligned}\mathbf{x}_{k+1} - \mathbf{x}_k &= (1 - l_k)(\boldsymbol{\xi} - \mathbf{x}_k - \beta_k \nabla f(\mathbf{x}_k) + \mathbf{u}_{l_k}(\mathbf{x}_k)) + (1 - l_k)O(\mathbf{y}_k - \mathbf{x}_k) \\ &= (1 - l_k)(\boldsymbol{\xi} - \mathbf{x}_k - \beta_k \nabla f(\mathbf{x}_k) + \mathbf{u}_{l_k}(\mathbf{x}_k)) + o(1 - l_k),\end{aligned}$$

where the second equality comes from the fact that $(1 - l_k)(\mathbf{y}_k - \mathbf{x}_k) = O((1 - l_k)^2) = o(1 - l_k)$ —multiplying both sides of eq. (7) by $1 - l_k$ and choose $\beta_k = O(1 - l_k)$ —as $1 - l_k \rightarrow 0$.

To derive a continuous-time limit for eq. (8), we introduce the *ansatz* $\mathbf{x}_k \approx X(t)$, where $X(t)$ is a smooth curve defined for $t \geq 0$. Let $\Delta t := 1 - l_k$ representing the stepsize for the k th iteration, then $X(t + \Delta t) \approx \mathbf{x}_{k+1}$. Therefore, as $1 - l_k \rightarrow 0$, eq. (8) becomes

$$(9) \quad X(t + \Delta t) - X(t) = \Delta t(-X(t) - \beta(t)\nabla f(X(t)) + \mathbf{u}_t(X(t))) + \sigma(t)(W(t + \Delta t) - W(t)),$$

where $W(t)$ is a standard Wiener process, $\beta(t)$ is a time-dependent coefficient corresponding to β_k , and $\mathbf{u}_t(X(t))$ is a time-dependent vector field corresponding to $\mathbf{u}_{l_k}(X(t))$, $\sigma(t)$ is the continuous analogy of $\sqrt{1 - l_k}$ arising from the Euler-Maruyama discretization of the SDE [24]. For simplicity, we denote $X(t)$ by X_t in the rest of this paper.

Notice that iterations eq. (4) converge when $\sum_{k=0}^{\infty}(1 - l_k) < +\infty$. This condition ensures that the cumulative step size $t = \sum_{i=0}^k(1 - l_i)$ converges to a finite limit T . We summarize the above derivation in the following proposition.

Proposition 3.0.1. *Let $X(t_0) = \mathbf{x}_K$ for some iteration number K , eq. (4) can be viewed as a discrete version of the following SDE for $0 < t_0 \leq t \leq T$:*

$$(10) \quad dX_t = \mathbf{b}_t(X_t)dt + \sigma(t)dW_t,$$

where $\mathbf{b}_t(X_t) = -X_t - \beta(t)\nabla f(X_t) + \mathbf{u}_t(X_t)$, $\mathbf{u}_t(X_t)$ is a time-dependent vector field associated to \mathbf{u}_{l_k} , and $\beta(t), \sigma(t) \in [0, 1)$ are monotonically non-increasing in t , and go to zeros.

Remark 2. *As the iteration number k increases, $1 - l_k \rightarrow 0$, but it remains insufficiently small in early iterations to ensure an accurate continuous approximation of the discrete process. Consequently, the iterative update in eq. (4) can be approximated by an SDE with an initial condition at some $t \geq t_0 > 0$, given by $X(t_0) = \mathbf{x}_K$. The SDE in eq. (10) accounts for the non-negligible step size in early iterations by starting the SDE at a positive time t_0 .*

4. ERROR AND CONVERGENCE ANALYSIS OF PNP-FLOW

4.1. Error Estimation. In image restoration applications, the ground truth vector field satisfying the ODE eq. (1) is only defined for each training data in a conditional fashion. The unknown marginal vector field $\mathbf{u}_t(\cdot)$ is approximated by a NN-parameterized vector field $\tilde{\mathbf{u}}_t(\cdot, \theta)$ —obtained by regressing against the conditional vector field using CFM [25]. Consequently, the error between the true restored \mathbf{x}^* and the approximated solution $\tilde{\mathbf{x}}^*$ obtained via the iteration eq. (4) comes from the gap between the vector fields \mathbf{u}_t and $\tilde{\mathbf{u}}_t$.

In this subsection, we aim to estimate the error $\epsilon = \|\mathbf{x}^* - \tilde{\mathbf{x}}^*\|$ and the convergence rate of PnP-Flow. Using the continuous counterpart, we seek to bound the expected error $\mathbb{E}[\|X_t - \tilde{X}_t\|]$. Consider the initial error $\epsilon_0 = \|\mathbf{x}_K - \tilde{\mathbf{x}}_K\|$, and the following pair of SDEs:

$$dX_t = \mathbf{b}_t(X_t)dt + \sigma(t)dW_t, \quad \text{and} \quad d\tilde{X}_t = \tilde{\mathbf{b}}_t(\tilde{X}_t)dt + \sigma(t)dW_t,$$

where $\tilde{\mathbf{b}}_t(\tilde{X}_t) = -\tilde{X}_t - \beta(t)\nabla f(\tilde{X}_t) + \tilde{\mathbf{u}}_t(\tilde{X}_t)$. We notice that eq. (10) admits a global unique solution [31] given $X(t_0) = \mathbf{x}_K$ under the following common mild assumptions [31, 39]:

Assumption 4.1.1 ([31][Theorem 5.2.1]). *Let $T > 0$ and $\mathbf{b}_t(X_t) : [0, T] \times \mathbb{R}^n \rightarrow \mathbb{R}^n$ and $\sigma(t) : \mathbb{R} \rightarrow \mathbb{R}$ be measurable functions satisfying $\|\mathbf{b}_t(X_t)\| + \sigma(t) \leq C_1(1 + \|X_t\|)$; $X_t \in \mathbb{R}^n$, $\forall t \in [0, T]$ for some constant C_1 , and $\|\mathbf{b}_t(X_t) - \mathbf{b}_t(Y_t)\| \leq C_2\|X_t - Y_t\|$ for some constant C_2 . Moreover, the initial condition satisfies $\mathbb{E}[\|X_{t_0}\|^2] < \infty$.*

To analyze the error term $\mathbb{E}[\|X_t - \tilde{X}_t\|]$, we further assume that

Assumption 4.1.2. *The learned vector field $\tilde{\mathbf{u}}_t(X_t)$ is bounded and Lipschitz continuous, i.e.,*

$$\|\tilde{\mathbf{u}}_s(X_s) - \tilde{\mathbf{u}}_t(X_t)\| \leq L_u\|X_s - X_t\|,$$

where L_u is the Lipschitz constant. Since $\tilde{\mathbf{u}}_t$ is an approximation of \mathbf{u}_t , we further assume that \mathbf{u}_t is also bounded and Lipschitz continuous with L_u .

Assumption 4.1.3. *$f(\cdot) : \mathbb{R}^n \rightarrow \mathbb{R}$ is a bounded twice differentiable function with a bounded Jacobian matrix, and $\nabla f(\cdot)$ is Lipschitz continuous. That is,*

$$\|\nabla f(X_t) - \nabla f(Y_t)\| \leq L_f\|X_t - Y_t\|, \quad \text{and} \quad \|\nabla f(X_t)\| \leq M_f,$$

where L_f is the Lipschitz constant for function f , and M_f is a positive constant.

The following theorem gives an upper bound for $\mathbb{E}[\|X_t - \tilde{X}_t\|]$:

Theorem 4.1.4. *Let X_t, \tilde{X}_t be the variables generated by eq. (10) with ground truth $\mathbf{u}_t(X_t)$ and learned vector $\tilde{\mathbf{u}}_t(\tilde{X}_t)$ fields at time t . Let $Z_t = X_t - \tilde{X}_t$, and $\epsilon_0 = \|X_{t_0} - \tilde{X}_{t_0}\| = \|\mathbf{x}_K - \tilde{\mathbf{x}}_K\|$. Under assumption 4.1.1, 4.1.2 and 4.1.3, we have*

$$(11) \quad \mathbb{E}[\|Z_t\|] \leq C_\epsilon e^{B_\epsilon},$$

where $C_\epsilon = \epsilon_0 + \int_{t_0}^t \mathbb{E}[\|\mathbf{u}_s(X_s) - \tilde{\mathbf{u}}_s(X_s)\|]ds$ and $B_\epsilon = \int_{t_0}^t (1 + \beta(s)L_f + L_u)ds$.

Proof.

$$(12) \quad \begin{aligned} \mathbb{E}[\|Z_t\|] &= \mathbb{E}[\|X_t - \tilde{X}_t\|] \\ &= \mathbb{E}[\|X_{t_0} - \tilde{X}_{t_0} + \int_{t_0}^t (\mathbf{b}_s(X_s) - \tilde{\mathbf{b}}_s(\tilde{X}_s))ds + \int_{t_0}^t \sigma(s) - \sigma(s)dW_s\|] \\ &\leq \epsilon_0 + \mathbb{E}[\|\int_{t_0}^t (\mathbf{b}_s(X_s) - \tilde{\mathbf{b}}_s(\tilde{X}_s))ds\|], \end{aligned}$$

where

$$\begin{aligned}
 & \mathbb{E}[\|\int_{t_0}^t (\mathbf{b}_s(X_s) - \tilde{\mathbf{b}}_s(\tilde{X}_s))ds\|] \\
 & \leq \mathbb{E}[\|\int_{t_0}^t (-X_s - \beta(s)\nabla f(X_s) + \mathbf{u}_s(X_s)) - (-\tilde{X}_s - \beta(s)\nabla f(\tilde{X}_s) + \tilde{\mathbf{u}}_s(\tilde{X}_s))ds\|] \\
 & = \mathbb{E}[\|\int_{t_0}^t (-(X_s - \tilde{X}_s) - \beta(s)(\nabla f(X_s) - \nabla f(\tilde{X}_s)) + (\mathbf{u}_s(X_s) - \tilde{\mathbf{u}}_s(\tilde{X}_s))ds\|] \\
 & \leq \mathbb{E}[\|\int_{t_0}^t \|(-(X_s - \tilde{X}_s) - \beta(s)(\nabla f(X_s) - \nabla f(\tilde{X}_s)) + (\mathbf{u}_s(X_s) - \tilde{\mathbf{u}}_s(\tilde{X}_s))\|ds\|] \\
 (13) \quad & \leq \mathbb{E}[\|\int_{t_0}^t \|X_s - \tilde{X}_s\| + \beta(s)\|\nabla f(X_s) - \nabla f(\tilde{X}_s)\| + \|\mathbf{u}_s(X_s) - \tilde{\mathbf{u}}_s(\tilde{X}_s)\|ds\|] \\
 & \leq \mathbb{E}[\|\int_{t_0}^t (1 + \beta(s)L_f)\|X_s - \tilde{X}_s\| + \|\mathbf{u}_s(X_s) - \tilde{\mathbf{u}}_s(X_s) + \tilde{\mathbf{u}}_s(X_s) - \tilde{\mathbf{u}}_s(\tilde{X}_s)\|ds\|] \\
 & \leq \mathbb{E}[\|\int_{t_0}^t (1 + \beta(s)L_f)\|X_s - \tilde{X}_s\| + \|\mathbf{u}_s(X_s) - \tilde{\mathbf{u}}_s(X_s)\| + \|\tilde{\mathbf{u}}_s(X_s) - \tilde{\mathbf{u}}_s(\tilde{X}_s)\|ds\|] \\
 & \leq \mathbb{E}[\|\int_{t_0}^t (1 + \beta(s)L_f + L_u)\|X_s - \tilde{X}_s\| + \|\mathbf{u}_s(X_s) - \tilde{\mathbf{u}}_s(X_s)\|ds\|] \\
 & = \int_{t_0}^t \mathbb{E}[\|\mathbf{u}_s(X_s) - \tilde{\mathbf{u}}_s(X_s)\|]ds + \int_{t_0}^t (1 + \beta(s)L_f + L_u)\mathbb{E}[\|Z_s\|]ds.
 \end{aligned}$$

Given the initial condition and $\tilde{\mathbf{u}}$, $\epsilon_0 + \int_{t_0}^t \mathbb{E}[\|\mathbf{u}_s(X_s) - \tilde{\mathbf{u}}_s(X_s)\|]ds$ can be treated as a constant, then applying Grönwall's inequality yields

$$\begin{aligned}
 & \mathbb{E}[\|Z_t\|] \leq C_\epsilon e^{B_\epsilon}, \\
 & \text{where } C_\epsilon = \epsilon_0 + \int_{t_0}^t \mathbb{E}[\|\mathbf{u}_s(X_s) - \tilde{\mathbf{u}}_s(X_s)\|]ds, \quad B_\epsilon = \int_{t_0}^t (1 + \beta(s)L_f + L_u)ds.
 \end{aligned}$$

This completes the proof. \square

eq. (11) implies that given a fixed function f , the error $\mathbb{E}[\|Z_t\|]$ is determined not only by the initial error ϵ_0 and the approximation error $\|\mathbf{u}_t(X_t) - \tilde{\mathbf{u}}_t(\tilde{X}_t)\|$, but also by L_u . Clearly, given a fixed $t \geq t_0$, ϵ_0 increases with the parameter t_0 (i.e. K), while C_ϵ and B_ϵ decrease as t_0 increases. We will verify the impact of K on the error bound empirically in Section 6.2.

4.2. Convergence Rates of PnP-Flow. Proposition 2.2.1—a convergence result established in [29]—only provides convergence for PnP-Flow without the convergence rate. By proposition 2.2.1, the sequence $\{\mathbf{x}_k\}$ generated by eq. (4) with $\tilde{\mathbf{b}}$ converges [29]. Let \mathbf{x}^* be the limit of the sequence $\{\mathbf{x}_k\}$, $X_T \approx \mathbf{x}^*$. Since $\sum_{k=0}^\infty (1 - l_k) \leq T$, we have $1 - l_k = 0$ when $t \geq T$, indicating that $\Delta t = 0$, $\beta(t) = 0$, and $\sigma(t) = 0$. Therefore, for $t \geq T$, $\tilde{\mathbf{b}}_T(X_T)dt + \sigma(t)dW_t = 0$. Define the function $\mathcal{E}(t) := \|X_t - X_T\|^2$, where X_T approximates \mathbf{x}^* of eq. (4) with $\tilde{\mathbf{b}}$, and X_T is also an approximate solution to eq. (2).

Theorem 4.2.1. *Under assumption 4.1.1, 4.1.2, and 4.1.3, the numerical solution X_T of eq. (10) with the initial condition X_{t_0} satisfies,*

$$(14) \quad \mathbb{E}[\|X_t - X_T\|^2] \leq A + 2\mathbb{E}[\int_{t_0}^t B(s)\|X_s - X_T\|^2ds], \forall t \geq t_0,$$

where $A = \mathbb{E}[\|X_{t_0} - X_T\|^2] + \int_{t_0}^t (n\sigma^2(s) + \frac{M_f^2\beta(s)}{2\eta})ds$, $\eta > 0$ and

$$B(s) = \begin{cases} -1 + L_u + \beta(s)L_f + \frac{\eta\beta(s)}{2}, & \text{if } f(\cdot) \text{ is Lipschitz differentiable with } L_f. \\ -1 + L_u + \frac{\eta\beta(s)}{2}, & \text{if } f(\cdot) \text{ is a convex function.} \\ -1 + L_u - \beta(s)\mu_f + \frac{\eta\beta(s)}{2}, & \text{if } f(\cdot) \text{ is a } \mu_f\text{-strongly convex function.} \end{cases}$$

Proof. Given any function $\mathcal{J}(t) = \mathcal{E}(t, X_t)$, applying the Ito's lemma to the SDE with $\tilde{\mathbf{b}}$ in eq. (10) gives

$$d(\mathcal{J}(t)) = [\partial_t \mathcal{E}(t, X_t) + \nabla \mathcal{E}(t, X_t) \cdot \tilde{\mathbf{b}}_t(X_t)]dt + \sigma(t)\nabla \mathcal{E}(t, X_t)dW_t + \frac{\sigma^2(t)}{2} \text{Trace}\{\nabla^2 \mathcal{E}(t, X_t)\}dt,$$

where the notation ∇ and ∇^2 , respectively, denote the Jacobian matrix and the Hessian matrix with respect to the space variable X_t .

Define the function $\mathcal{E}(t, X_t) := \|X_t - X_T\|^2$, the Ito's lemma gives

$$(15) \quad d(\mathcal{E}(t, X_t)) = 2\langle X_t - X_T, \tilde{\mathbf{b}}_t(X_t) \rangle dt + 2\sigma(t)\langle X_t - X_T, dW_t \rangle + n\sigma^2(t)dt.$$

Substitute $\tilde{\mathbf{b}}_T(X_T)dt + \sigma(T)dW_T = 0$, we have

$$d(\mathcal{E}(t, X_t)) = 2\langle X_t - X_T, \tilde{\mathbf{b}}_t(X_t) - \tilde{\mathbf{b}}_T(X_T) \rangle dt + 2(\sigma(t) - \sigma(T))\langle X_t - X_T, dW_t \rangle + n\sigma^2(t)dt.$$

Taking its integral form, we have

$$(16) \quad \begin{aligned} \mathbb{E}[\mathcal{E}(t, X_t)] &= \mathbb{E}[\|X_{t_0} - X_T\|^2] + 2 \int_{t_0}^t \langle X_s - X_T, \tilde{\mathbf{b}}_s(X_s) - \tilde{\mathbf{b}}_T(X_T) \rangle + n\sigma^2(s)ds \\ &\quad + 2 \int_{t_0}^t (\sigma(s) - \sigma(T))\langle X_s - X_T, dW_t \rangle] \\ &= \mathbb{E}[\|X_{t_0} - X_T\|^2] + \mathbb{E}[\int_{t_0}^t 2\langle X_s - X_T, \tilde{\mathbf{b}}_s(X_s) - \tilde{\mathbf{b}}_T(X_T) \rangle + n\sigma^2(s)ds] \\ &= \mathbb{E}[\|X_{t_0} - X_T\|^2] + n \int_{t_0}^t \sigma^2(s)ds + 2\mathbb{E}[\int_{t_0}^t \langle X_s - X_T, \tilde{\mathbf{b}}_s(X_s) - \tilde{\mathbf{b}}_T(X_T) \rangle ds], \end{aligned}$$

and

$$(17) \quad \begin{aligned} &\langle X_s - X_T, \tilde{\mathbf{b}}_s(X_s) - \tilde{\mathbf{b}}_T(X_T) \rangle \\ &= \langle X_s - X_T, -X_s - \beta(s)\nabla f(X_s) + \tilde{\mathbf{u}}_s(X_s) + X_T + \beta(T)\nabla f(X_T) - \tilde{\mathbf{u}}_T(X_T) \rangle \\ &= -\|X_s - X_T\|^2 - \beta(s)\langle X_s - X_T, \nabla f(X_s) - \nabla f(X_T) \rangle - \beta(s)\langle X_s - X_T, \nabla f(X_T) \rangle \\ &\quad + \langle X_s - X_T, \tilde{\mathbf{u}}_s(X_s) - \tilde{\mathbf{u}}_T(X_T) \rangle \\ &\leq -\|X_s - X_T\|^2 + \|X_s - X_T\| \|\tilde{\mathbf{u}}_s(X_s) - \tilde{\mathbf{u}}_T(X_T)\| \\ &\quad - \beta(s)\langle X_s - X_T, \nabla f(X_s) - \nabla f(X_T) \rangle - \beta(s)\langle X_s - X_T, \nabla f(X_T) \rangle \\ &\leq (-1 + L_u)\|X_s - X_T\|^2 - \beta(s)\langle X_s - X_T, \nabla f(X_s) - \nabla f(X_T) \rangle \\ &\quad + \beta(s)\|X_s - X_T\| \|\nabla f(X_T)\| \\ &\leq (-1 + L_u)\|X_s - X_T\|^2 - \beta(s)\langle X_s - X_T, \nabla f(X_s) - \nabla f(X_T) \rangle \\ &\quad + \beta(s)(\frac{\eta}{2}\|X_s - X_T\|^2 + \frac{M_f^2}{2\eta}) \end{aligned}$$

where $\eta > 0$ is an arbitrary positive number by Young's inequality. The upper bound of $\langle X_s - X_T, \tilde{\mathbf{b}}_s(X_s) - \tilde{\mathbf{b}}_T(X_T) \rangle$ depends on the property of $f(\cdot)$ as follows

- (i) When f is nonconvex but Lipschitz differentiable with Lipschitz constant L_f and have bounded gradient $\|\nabla f(X_t)\| \leq M_f$, such that

$$-L_f\|X_s - X_T\|^2 \leq \langle X_s - X_T, \nabla f(X_s) - \nabla f(X_T) \rangle \leq L_f\|X_s - X_T\|^2,$$

then

$$(18) \quad \langle X_s - X_T, \tilde{\mathbf{b}}_s(X_s) - \tilde{\mathbf{b}}_T(X_T) \rangle \leq (-1 + L_u + \beta(s)L_f + \frac{\eta\beta(s)}{2})\|X_s - X_T\|^2 + \frac{M_f^2\beta(s)}{2\eta}$$

- (ii) When f is a convex function such that

$$\langle X_s - X_T, \nabla f(X_s) - \nabla f(X_T) \rangle \geq 0,$$

we have

$$(19) \quad \langle X_s - X_T, \tilde{\mathbf{b}}_s(X_s) - \tilde{\mathbf{b}}_T(X_T) \rangle \leq (-1 + L_u + \frac{\eta\beta(s)}{2})\|X_s - X_T\|^2 + \frac{M_f^2\beta(s)}{2\eta}.$$

- (iii) When f is a μ_f -strongly convex function, such that

$$\langle X_s - X_T, \nabla f(X_s) - \nabla f(X_T) \rangle \geq \mu_f\|X_s - X_T\|^2,$$

we get

$$(20) \quad \langle X_s - X_T, \tilde{\mathbf{b}}_s(X_s) - \tilde{\mathbf{b}}_T(X_T) \rangle \leq (-1 + L_u - \beta(s)\mu_f + \frac{\eta\beta(s)}{2})\|X_s - X_T\|^2 + \frac{M_f^2\beta(s)}{2\eta}$$

In summary, let $B(s)$ be the coefficient of $\|X_s - X_T\|^2$, we have

$$(21) \quad B(s) = \begin{cases} -1 + L_u + \beta(s)L_f + \frac{\eta\beta(s)}{2}, & \text{if } f(\cdot) \text{ is Lipschitz differentiable with } L_f. \\ -1 + L_u + \frac{\eta\beta(s)}{2}, & \text{if } f(\cdot) \text{ is a convex function.} \\ -1 + L_u - \beta(s)\mu_f + \frac{\eta\beta(s)}{2}, & \text{if } f(\cdot) \text{ is a } \mu_f\text{-strongly convex function.} \end{cases}$$

It is evident that: i) when f is not a strongly convex function, $0 < L_u < 1$ is a necessary condition for $B(s) < 0$, $\forall s \in [t_0, t]$; ii) when f is a strongly convex function, $B(s) < 0$ as long as $0 \leq L_u < 1 + \beta(s)\mu_f - \frac{\eta\beta(s)}{2}$. The strong convexity of f allows $\tilde{\mathbf{u}}$ to be potentially non-contractive.

Let $A = \mathbb{E}[\|X_{t_0} - X_T\|^2] + \int_{t_0}^t (n\sigma^2(s) + \frac{M_f^2\beta(s)}{2\eta})ds$, we have

$$(22) \quad \mathbb{E}[\|X_t - X_T\|^2] \leq A + 2\mathbb{E}[\int_{t_0}^t B(s)\|X_s - X_T\|^2 ds].$$

The sign of $B(s)$ depends on L_u , $\beta(s)$, and the properties of $f(\cdot)$. However, for fixed L_u and $f(\cdot)$, since $\beta(s)$ is monotonically non-increasing, $B(s)$ is also a monotonic function. $B(s)$ is monotonically non-increasing when f is a Lipschitz differentiable function or a convex function.

This completes the proof. \square

According to eq. (14), the convergence rate is directly influenced by $\sigma(t)$ and $\beta(t)$, both of which are controlled by the step schedule $1 - l_k$, as well as by the Lipschitz constant L_u and the initial condition X_{t_0} .

5. SDE INFORMED IMPROVEMENT FOR PNP-FLOW

In this section, we present a few strategies to improve PnP-Flow based on the theoretical results established in Section 4.

5.1. A New Schedule for $1 - l_k$. The convergence of both eq. (4) and eq. (24)—our proposed accelerated PnP-Flow—relies on the assumption that $\sum_{k=0}^{\infty} (1 - l_k) < +\infty$, which requires $\{1 - l_k\}$ to be a convergent sequence. However, in the implementation of [29], l_k is defined as $l_k = \frac{k}{N}$, where N is the total number of iterations. Although such an implementation provides good numerical results, this choice leads to $1 - l_k = \frac{N-k}{N} \geq \frac{1}{N}$, $\forall k \leq N$, where $\sum_{N=1}^{\infty} \frac{1}{N}$ diverges—contradicting the convergence assumption.

To address this issue, we propose an alternative form for l_k that ensures $\sum_{k=0}^{\infty} (1 - l_k)$ converges:

$$(23) \quad l_k = 1 - \lambda^k, \quad \lambda \in (0, 1).$$

Here, the sequence $\{1 - l_k\} = \{\lambda^k\}$ is geometrically decreasing, and its sum evaluates to: $\sum_{k=0}^{\infty} \lambda^k = \frac{1}{1-\lambda} < +\infty$. The selection of an appropriate λ depends on the total iteration count N , and λ^k converges to zero as $k \rightarrow N$. Excessively small λ results in a large step size $1 - l_k$, and it decays too rapidly to zero, increasing the local truncation error, as well as exacerbating the accumulation of numerical errors. For overly large λ , the final term λ^N fails to approach zero, violating our convergence conditions. Furthermore, our proposed schedule strategically allocates more iterations to smaller $1 - l_k$ values, enhancing the generation of fine details.

5.2. Lipschitz Regularization. In theorem 4.1.4, for a fixed t_0 , B_ϵ increases with L_u , indicating that penalizing the Lipschitz constant of $\tilde{\mathbf{u}}_t$ helps suppress the overall error. The idea of penalizing the Lipschitz constant of NNs has been widely explored (e.g., in training Wasserstein GANs [2, 14, 30]). In our experiments, we adopt the approach from [14]. The output of the vector field regressor $\tilde{\mathbf{u}}_t(\tilde{X}_t)$ has the same dimension as its input, whereas the discriminator network in WGAN [14] produces a scalar output. Consequently, we penalize the Jacobian norm instead of the gradient norm for $\tilde{\mathbf{u}}_t(\tilde{X}_t)$, and computing the Jacobian of $\tilde{\mathbf{u}}_t(X_t)$ requires n gradient evaluations, where n is the data dimension. To improve computational and memory efficiency, we employ Hutchinson’s method [18, 27, 16] to estimate the Frobenius norm of the Jacobian $\nabla \tilde{\mathbf{u}}_t(\tilde{X}_t)$ whose supremum provides an upper bound of the Lipschitz constant. This approach provides an unbiased estimator; see Appendix A for details.

5.3. Acceleration via Extrapolation. Now we consider accelerating off-the-shelf PnP-Flow models without retraining. In particular, we consider an accelerated version of eq. (4) via extrapolation, which is given as follows:

$$(24) \quad \begin{cases} \mathbf{w}_k = \mathbf{x}_k + h_k(\mathbf{x}_k - \mathbf{x}_{k-1}), \\ \mathbf{z}_k = \mathbf{w}_k - \gamma_k \nabla f(\mathbf{w}_k), \\ \mathbf{y}_k = (1 - l_k)\boldsymbol{\xi} + l_k \mathbf{z}_k, \\ \mathbf{x}_{k+1} = D_{l_k}(\mathbf{y}_k), \end{cases}$$

where $\gamma_k, l_k, h_k \in (0, 1)$ are manually set parameters. We stress that the vector field in D_{l_k} is inherited from eq. (4) without restraining or fine-tuning. In the rest of this subsection, we will study the convergence rate of eq. (24) and compare it against that of eq. (4).

Proposition 5.3.1. *Assume that $f : \mathbb{R}^n \rightarrow \mathbb{R}$ is a differentiable function with bounded gradient, and the learned vector field $\tilde{\mathbf{u}}_t : [0, 1] \times \mathbb{R}^n \rightarrow \mathbb{R}^n$ is bounded and Lipschitz. Let the time sequence $\{l_k\}_{k \in \mathbb{N}}$ satisfy $l_k \in [0, 1]$, $\sum_{k=0}^{\infty} (1 - l_k) < +\infty$, and let $\gamma_k \leq 1 - l_k$. If the sequence $\{\mathbf{x}_k\}_{k \in \mathbb{N}}$ obtained by eq. (24) is bounded, then $h_k \in [0, \zeta]$ for some $\zeta \in (0, 1)$ is a necessary condition for the convergence of the sequence $\{\mathbf{x}_k\}_{k \in \mathbb{N}}$.*

Proof. By the iteration eq. (24) and the definition of D_{l_k} , we have

$$\begin{aligned}
 & \mathbf{x}_{k+1} - \mathbf{x}_k \\
 &= D_{l_k}(\mathbf{y}_k) - \mathbf{x}_k \\
 (25) \quad &= \mathbf{y}_k + (1 - l_k)\mathbf{u}_{l_k}(\mathbf{y}_k) - \mathbf{x}_k \\
 &= (1 - l_k)\boldsymbol{\xi} + l_k(\mathbf{w}_k - \gamma_k \nabla f(\mathbf{w}_k)) + (1 - l_k)\mathbf{u}_{l_k}(\mathbf{y}_k) - \mathbf{x}_k \\
 &= (1 - l_k)(\boldsymbol{\xi} - \mathbf{x}_k) + l_k h_k(\mathbf{x}_k - \mathbf{x}_{k-1}) - l_k \gamma_k \nabla f(\mathbf{w}_k) + (1 - l_k)\mathbf{u}_{l_k}(\mathbf{y}_k).
 \end{aligned}$$

Then

$$\begin{aligned}
 & \|\mathbf{x}_{k+1} - \mathbf{x}_k\| \\
 (26) \quad &= \|(1 - l_k)(\boldsymbol{\xi} - \mathbf{x}_k) + l_k h_k(\mathbf{x}_k - \mathbf{x}_{k-1}) - l_k \gamma_k \nabla f(\mathbf{w}_k) + (1 - l_k)\mathbf{u}_{l_k}(\mathbf{y}_k)\| \\
 &\leq (1 - l_k)(\|\boldsymbol{\xi} - \mathbf{x}_k + \mathbf{u}_{l_k}(\mathbf{y}_k)\| + l_k \|\nabla f(\mathbf{w}_k)\|) + l_k h_k \|\mathbf{x}_k - \mathbf{x}_{k-1}\| \\
 &\leq (1 - l_k)(\|\boldsymbol{\xi} - \mathbf{x}_k + \mathbf{u}_{l_k}(\mathbf{y}_k)\| + \|\nabla f(\mathbf{w}_k)\|) + h_k \|\mathbf{x}_k - \mathbf{x}_{k-1}\|
 \end{aligned}$$

Since $\boldsymbol{\xi}, \mathbf{x}_k, \mathbf{u}_{l_k}(\mathbf{y}_k)$ are all bounded by the assumption, there exists a constant $M > 0$, such that

$$(27) \quad \|\mathbf{x}_{k+1} - \mathbf{x}_k\| \leq (1 - l_k)M + h_k \|\mathbf{x}_k - \mathbf{x}_{k-1}\|.$$

Therefore,

$$(28) \quad \|\mathbf{x}_{k+1} - \mathbf{x}_k\| + \sum_{k=1}^{\infty} (1 - h_k) \|\mathbf{x}_k - \mathbf{x}_{k-1}\| \leq M \sum_{k=1}^{\infty} (1 - l_k) < +\infty.$$

The above inequality is trivial when $h_k \geq 1$. When $h_k \in [0, \zeta]$ for some $\zeta \in (0, 1)$ and $\sum_{k=1}^{\infty} (1 - l_k) < +\infty$, we have

$$(29) \quad \sum_{k=1}^{\infty} \|\mathbf{x}_{k+1} - \mathbf{x}_k\| \leq \frac{M}{1 - \zeta} \sum_{k=1}^{\infty} (1 - l_k) + \zeta \|\mathbf{x}_{k+1} - \mathbf{x}_k\| < +\infty,$$

which indicates that $\{\mathbf{x}_k\}$ is a Cauchy sequence and converges. This completes the proof. \square

Remark 3. The extrapolation coefficient h_k in proximal gradient methods has been extensively studied in both convex and nonconvex settings [33, 42, 46, 19]. Since eq. (24) can be interpreted as an inexact proximal gradient descent iteration in a nonconvex setting, the admissible range of h_k is more restricted than in convex scenarios. In the experimental section, we start with a small value of h_k and gradually increase it until the iteration fails to converge.

Proposition 5.3.2. The SDE counterpart of eq. (24) is given by the following SDE:

$$(30) \quad dX_t = \frac{\mathbf{b}_t(X_t)}{1 - \alpha(t)} dt + \frac{\sigma(t)}{1 - \alpha(t)} dW_t,$$

where $\mathbf{b}_t(X_t) = -X_t - \beta(t)\nabla f(X_t) + \mathbf{u}_t(X_t)$, $\alpha(t) \geq 0$, $\sigma(t) \in [0, 1]$. eq. (30) is in fact a rescaled version of eq. (10) with the scaling factor $\frac{1}{1 - \alpha(t)}$. eq. (24) is more precisely approximated by eq. (30) as the dynamic step size $1 - l_k$ goes to zero.

Proof. Clearly, we have

$$\begin{aligned}
 & \mathbf{x}_{k+1} - \mathbf{x}_k \\
 (31) \quad &= (1 - l_k)(\boldsymbol{\xi} - \mathbf{x}_k) + l_k h_k(\mathbf{x}_k - \mathbf{x}_{k-1}) - l_k \gamma_k \nabla f(\mathbf{w}_k) + (1 - l_k)\mathbf{u}_{l_k}(\mathbf{y}_k),
 \end{aligned}$$

and

$$(32) \quad \nabla f(\mathbf{w}_k) = \nabla f(\mathbf{x}_k) + \nabla^2 f(\mathbf{x}_k) h_k(\mathbf{x}_k - \mathbf{x}_{k-1}) + o(h_k(\mathbf{x}_k - \mathbf{x}_{k-1})),$$

$$\begin{aligned}
 \mathbf{u}_{l_k}(\mathbf{y}_k) &= \mathbf{u}_{l_k}(\mathbf{x}_k) + \nabla \mathbf{u}_{l_k}(\mathbf{x}_k)(\mathbf{y}_k - \mathbf{x}_k) + o(\mathbf{y}_k - \mathbf{x}_k), \\
 (33) \quad \text{where } \mathbf{y}_k - \mathbf{x}_k &= (1 - l_k)\boldsymbol{\xi} + l_k \mathbf{z}_k - \mathbf{x}_k \\
 &= (1 - l_k)(\boldsymbol{\xi} - \mathbf{x}_k) + l_k h_k(\mathbf{x}_k - \mathbf{x}_{k-1}) - l_k \gamma_k \nabla f(\mathbf{w}_k).
 \end{aligned}$$

When selecting sufficiently small γ_k, h_k such that $(1 - l_k)(\mathbf{y}_k - \mathbf{x}_k) = o(1 - l_k)$ and $\gamma_k h_k = o(1 - l_k)$, then combine eqs. (31) to (33) together, we have

$$\begin{aligned}
 \mathbf{x}_{k+1} - \mathbf{x}_k &= (1 - l_k)(\boldsymbol{\xi} - \mathbf{x}_k) + l_k h_k(\mathbf{x}_k - \mathbf{x}_{k-1}) - l_k \gamma_k \nabla f(\mathbf{w}_k) + (1 - l_k)\mathbf{u}_{l_k}(\mathbf{y}_k) \\
 (34) \quad &= (1 - l_k)(\boldsymbol{\xi} - \mathbf{x}_k) + l_k h_k(\mathbf{x}_k - \mathbf{x}_{k-1}) - l_k \gamma_k (\nabla f(\mathbf{x}_k) + \nabla^2 f(\mathbf{x}_k) h_k(\mathbf{x}_k - \mathbf{x}_{k-1})) \\
 &\quad - l_k \gamma_k o(h_k(\mathbf{x}_k - \mathbf{x}_{k-1})) + (1 - l_k)(\mathbf{u}_{l_k}(\mathbf{x}_k) + \nabla \mathbf{u}_{l_k}(\mathbf{x}_k)(\mathbf{y}_k - \mathbf{x}_k) + o(\mathbf{y}_k - \mathbf{x}_k)) \\
 &= (1 - l_k)(\boldsymbol{\xi} - \mathbf{x}_k) + l_k h_k(\mathbf{x}_k - \mathbf{x}_{k-1}) - l_k \gamma_k \nabla f(\mathbf{x}_k) + (1 - l_k)\mathbf{u}_{l_k}(\mathbf{x}_k) + o(1 - l_k).
 \end{aligned}$$

Set $\beta_k = \frac{l_k \gamma_k}{1 - l_k}$, we have

$$(35) \quad \mathbf{x}_{k+1} - \mathbf{x}_k = (1 - l_k)(\boldsymbol{\xi} - \mathbf{x}_k - \beta_k \nabla f(\mathbf{x}_k) + \mathbf{u}_{l_k}(\mathbf{x}_k)) + l_k h_k(\mathbf{x}_k - \mathbf{x}_{k-1}) + o(1 - l_k)$$

Again, introducing *Ansatz* $\mathbf{x}_k \approx X_t$ where X_t is a smooth curve defined for $t \geq 0$. As the step size $1 - l_k \rightarrow 0$, we have $X_t \approx \mathbf{x}_k$, $X(t + 1 - l_k) \approx \mathbf{x}_{k+1}$, $X(t - (1 - l_{k-1})) \approx \mathbf{x}_{k-1}$. And Taylor expansion gives

$$\begin{aligned}
 \mathbf{x}_{k+1} - \mathbf{x}_k &= (1 - l_k)\dot{X}(t) + o(1 - l_k) \\
 (36) \quad \mathbf{x}_k - \mathbf{x}_{k-1} &= (1 - l_{k-1})\dot{X}(t) + o(1 - l_{k-1})
 \end{aligned}$$

Therefore,

$$\begin{aligned}
 ((1 - l_k) - l_k h_k(1 - l_{k-1}))\dot{X}(t) \\
 (37) \quad &= (1 - l_k)(\boldsymbol{\xi} - X(t) - \beta_k \nabla f(X(t)) + \mathbf{u}_{l_k}(X(t))) + o(1 - l_k) + o(1 - l_{k-1})
 \end{aligned}$$

Set $\alpha_k = \frac{l_k h_k(1 - l_{k-1})}{1 - l_k}$, when $1 - l_k \rightarrow 0$, we get

$$(38) \quad (1 - \alpha_k)\dot{X}(t) = \boldsymbol{\xi} - X(t) - \beta_k \nabla f(X(t)) + \mathbf{u}_{l_k}(X(t)).$$

Replacing $\alpha_k, \beta_k, X(t)$ with $\alpha(t), \beta(t), X_t$, and introducing $\sigma(t)$ yields

$$(39) \quad dX_t = \frac{\mathbf{b}_t(X_t)}{1 - \alpha(t)} dt + \frac{\sigma(t)}{1 - \alpha(t)} dW_t,$$

where $\mathbf{b}_t(X_t) = -X_t - \beta(t)\nabla f(X_t) + \mathbf{v}(t, X_t)$. The above SDE is in fact a recaled version of eq. (10) with the scaling factor $\frac{1}{1 - \alpha(t)} \cdot \frac{1}{1 - \alpha(t)}$ increase with h_k , however, to ensure the convergence of the sequence $\{\mathbf{x}_k\}$, h_k can be sufficiently small but it is upper bounded.

This completes the proof. \square

Remark 4. Since we set $\alpha_k = \frac{l_k h_k(1 - l_{k-1})}{1 - l_k}$, the range of α_k directly depends on the value of h_k and the schedule for $1 - l_k$. In the setting in eq. (23), we see that $\alpha_k = \frac{1 - \lambda^k}{\lambda} h_k$. When selecting proper $0 \ll \lambda < 1$ and $0 \leq h_k \ll 1$, we can ensure that $0 \leq \alpha_k < 1$.

Theorem 5.3.3. Under assumption 4.1.1 and 4.1.2, the solution X_T of eq. (30) with the initial condition X_{t_0} satisfies,

$$(40) \quad \mathbb{E}[\|\mathbf{x}_t - \mathbf{x}_T\|^2] \leq A_\alpha + 2\mathbb{E}\left[\int_{t_0}^t \frac{B(s)}{1 - \alpha(s)} \|\mathbf{x}_s - \mathbf{x}_T\|^2 ds\right], \quad \forall t \geq t_0,$$

where $A_\alpha = \mathbb{E}[\|X_{t_0} - X_T\|^2] + \int_{t_0}^t \frac{n\sigma^2(s) + \frac{M_f^2\beta(s)}{2\eta}}{(1-\alpha(s))^2} ds$ and

$$B(s) = \begin{cases} -1 + L_u + \beta(s)L_f + \frac{\eta\beta(s)}{2}, & \text{if } f(\cdot) \text{ is Lipschitz differentiable with } L_f. \\ -1 + L_u + \frac{\eta\beta(s)}{2}, & \text{if } f(\cdot) \text{ is a convex function.} \\ -1 + L_u - \beta(s)\mu_f + \frac{\eta\beta(s)}{2}, & \text{if } f(\cdot) \text{ is a } \mu_f\text{-strongly convex function.} \end{cases}$$

Proof. Define the function $\mathcal{E}(t, X_t) := \|X_t - X_T\|^2$, taking the integral form, we have

$$(41) \quad \begin{aligned} \mathbb{E}[\mathcal{E}(t, X_t)] &= \mathbb{E}[\|X_{t_0} - X_T\|^2] + \int_{t_0}^t \frac{n\sigma^2(s)}{(1-\alpha(s))^2} ds \\ &\quad + 2\mathbb{E}\left[\int_{t_0}^t \frac{1}{1-\alpha(s)} \langle X_s - X_T, \tilde{\mathbf{b}}_s(X_s) - \tilde{\mathbf{b}}_T(X_T) \rangle ds\right], \end{aligned}$$

and

$$(42) \quad \begin{aligned} &\langle X_s - X_T, \tilde{\mathbf{b}}_s(X_s) - \tilde{\mathbf{b}}_T(X_T) \rangle \\ &\leq (-1 + L_u)\|X_s - X_T\|^2 - \beta(s)\langle X_s - X_T, \nabla f(X_s) - \nabla f(X_T) \rangle \\ &\quad + \beta(s)\left(\frac{\eta}{2}\|X_s - X_T\|^2 + \frac{M_f^2}{2\eta}\right). \end{aligned}$$

Let $A_\alpha = \mathbb{E}[\|X_{t_0} - X_T\|^2] + \int_{t_0}^t \frac{n\sigma^2(s) + \frac{M_f^2\beta(s)}{2\eta}}{(1-\alpha(s))^2} ds$ we have

$$(43) \quad \mathbb{E}[\|X_t - X_T\|^2] \leq A_\alpha + 2\mathbb{E}\left[\int_{t_0}^t \frac{B(s)}{1-\alpha(s)} \|X_s - X_T\|^2 ds\right].$$

This completes the proof. \square

The upper bound in eq. (14) becomes nontrivial when $\int_{t_0}^t B(s)\|X_s - X_T\|^2 ds < 0$. Under the same setting, when $\alpha(t)$ is a constant $\alpha \in [0, 1)$, it is easy to verify that $\frac{1}{1-\alpha} \int_{t_0}^t B(s)\|X_s - X_T\|^2 ds \leq \int_{t_0}^t B(s)\|X_s - X_T\|^2 ds$, since $\frac{1}{1-\alpha} \geq 1$. This shows that the extrapolation step in eq. (24) permits a wider admissible range of values for $B(s)$ such that the upper bound remains nontrivial, thereby relaxing the conditions required on f . In practice, we can select proper $\beta(t)$ and $\alpha(t)$ such that $\frac{B(s)}{1-\alpha(s)}$ is the dominant term determining the magnitude of the upper bound, as well as the convergence rate, leading to smaller $\|X_t - X_T\|^2$.

6. NUMERICAL EXPERIMENTS

In this section, we validate the performance of our improved PnP-Flow (IPnP-Flow) method—as laid out in Section 5—using several benchmark image restoration tasks. The numerical experiments also aim to solidify our established theoretical analysis of PnP-Flow. We compare IPnP-Flow with baseline methods for various image restoration tasks in Section 6.1, and we perform ablation studies to investigate the effects of each additional component of IPnP-Flow over PnP-Flow in Section 6.2. Additional experimental details and results are presented in section A.

Experiment Setup: Our implementation is based on the codes provided in the paper [29] using PyTorch. All experiments are conducted on NVIDIA RTX 4090 GPUs. Training details and hyperparameters for different tasks are available in the section A. For each task, we conduct five independent runs with different random seeds and report the mean performance \pm standard deviation.

Image Restoration Tasks: The experiments focus on denoising, deblurring, super-resolution, and inpainting tasks, conducted on two widely adopted datasets: CelebA [47] and AFHQ-Cat [8]. To ensure a fair comparison with PnP-Flow (the baseline our work primarily improves upon), we

adopt identical experimental settings from [29], including dataset splits (training/validation/test), model architectures, task settings, and evaluation protocols.

Baseline Methods: We compare our approach against the original PnP-Flow [29] and other SOTA methods, including OT-ODE [34], D-Flow [4], Flow priors [51], PnP-Diff [52], and PnP-FBS [17], demonstrating improvements in restoration quality and efficiency.

Clean	Degraded	PnP-GS	OT-ODE	Flow-Priors	PnP-Flow	Ours
Denoising	PSNR: 19.97	PSNR: 31.86	PSNR: 29.48	PSNR: 28.30	PSNR: 30.95	PSNR: 32.25
Deblurring	PSNR: 26.75	PSNR: 34.33	PSNR: 33.33	PSNR: 31.59	PSNR: 34.93	PSNR: 35.98
Super-resolution	PSNR: 8.98	PSNR: 30.57	PSNR: 34.31	PSNR: 29.01	PSNR: 32.25	PSNR: 34.56
Rand. Inpainting	PSNR: 13.09	PSNR: 29.06	PSNR: 28.70	PSNR: 32.78	PSNR: 33.51	PSNR: 34.72
Box Inpainting	PSNR: 20.58	PSNR: N/A	PSNR: 31.95	PSNR: 32.61	PSNR: 32.39	PSNR: 33.81

FIGURE 1. Comparison of image restoration methods on CelebA.

6.1. Image Restoration Results. We present quantitative results in table 1 (CelebA) and table 2 (AFHQ-Cat), reporting PSNR and SSIM averaged over 100 test images per task. For competing methods, we directly adopt the best-reported results from [29], where hyperparameters (including task-specific iteration numbers ranging from 100 to 500) were meticulously optimized. In contrast, our IPnP-Flow uses a fixed 100 iterations across all tasks. Despite this conservative setup, IPnP-Flow consistently outperforms PnP-Flow and other baselines, demonstrating the efficacy of our SDE-informed enhancements. While higher iterations could further improve results, our method achieves superior performance with greater efficiency.

Our method achieves superior PSNR and SSIM scores across all tasks and datasets compared to PnP-Flow, with gains of up to 2.17 dB in PSNR (CelebA Super-resolution) and 0.79 dB (AFHQ-Cat denoising). These improvements stem from the SDE model’s guidance on error reduction and

TABLE 1. Performance (PSNR/SSIM) on CelebA Dataset

Method	Denoising	Deblurring	Super-resolution	Random Inpainting	Box Inpainting
Degraded	20.00 / 0.348	27.67 / 0.740	7.527 / 0.012	11.82 / 0.197	22.12 / 0.742
OT-ODE	30.50 / 0.867	32.63 / 0.915	31.05 / 0.902	28.36 / 0.865	28.84 / 0.914
D-Flow	26.42 / 0.651	31.07 / 0.877	30.75 / 0.866	33.07 / 0.938	29.70 / 0.893
Flow-Priors	29.26 / 0.766	31.40 / 0.856	28.35 / 0.717	32.33 / 0.945	29.40 / 0.858
PnP-Diff	31.00 / 0.883	32.49 / 0.911	31.20 / 0.893	31.43 / 0.917	N/A
PnP-GS	32.45 / 0.908	33.65 / 0.924	30.69 / 0.889	28.45 / 0.848	N/A
PnP-Flow	<u>32.45 / 0.911</u>	<u>34.51 / 0.940</u>	<u>31.49 / 0.907</u>	<u>33.54 / 0.953</u>	<u>30.59 / 0.943</u>
Ours (PSNR)	33.31 \pm 0.07	35.13 \pm 0.08	33.66 \pm 0.16	34.65 \pm 0.04	30.93 \pm 0.05
Ours (SSIM)	0.927 \pm 0.003	0.951 \pm 0.002	0.946 \pm 0.003	0.965 \pm 0.001	0.953 \pm 0.001

TABLE 2. Performance (PSNR/SSIM) on AFHQ-Cat Dataset

Method	Denoising	Deblurring	Super-resolution	Random Inpainting	Box Inpainting
Degraded	20.00 / 0.319	23.77 / 0.514	10.74 / 0.042	13.35 / 0.234	21.50 / 0.744
OT-ODE	29.90 / 0.831	26.43 / 0.709	25.17 / 0.711	28.84 / 0.838	23.88 / 0.874
D-Flow	26.22 / 0.620	27.49 / 0.740	24.10 / 0.595	31.37 / 0.888	26.69 / 0.833
Flow-Priors	29.32 / 0.768	25.78 / 0.692	23.34 / 0.573	31.76 / 0.909	25.85 / 0.822
PnP-Diff	30.27 / 0.835	<u>27.97 / 0.764</u>	23.22 / 0.601	31.08 / 0.882	N/A
PnP-GS	<u>32.26 / 0.895</u>	<u>27.33 / 0.749</u>	21.86 / 0.619	29.61 / 0.855	N/A
PnP-Flow	31.65 / 0.876	27.62 / 0.763	<u>26.75 / 0.774</u>	<u>32.98 / 0.930</u>	<u>26.87 / 0.904</u>
Ours (PSNR)	32.44 \pm 0.13	28.15 \pm 0.06	27.38 \pm 0.04	33.21 \pm 0.04	27.01 \pm 0.05
Ours (SSIM)	<u>0.894</u> \pm 0.003	0.780 \pm 0.004	0.796 \pm 0.003	0.937 \pm 0.001	0.908 \pm 0.002

acceleration. Qualitative results (see fig. 1) further illustrate that our method produces sharper, artifact-free restorations compared to baselines, enhancing visual fidelity.

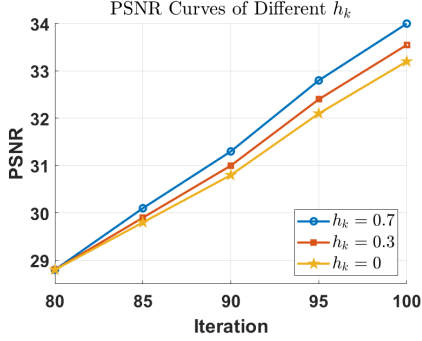
Our improved PnP-Flow maintains nearly identical computational efficiency to the original PnP-Flow during inference, as the model architecture is unchanged. The additional extrapolation step has minimal impact on computation time, with the dominant cost still coming from denoising steps.

6.2. Ablation Study. The performance of IPnP-Flow, particularly its error bound and convergence rate, is governed by three principal factors: (1) the extrapolation step size h_k , (2) the schedule of $1 - l_k$, and (3) the Lipschitz constant L_u . We conduct a systematic empirical analysis on the CelebA validation dataset to investigate their individual effects.

Extrapolation Step Size h_k : The upper bound in theorem 5.3.3 for $\mathbb{E}[\|X_t - X_T\|^2]$ depends critically on h_k . Since X_T approximates the ground truth $X_G \in \mathbb{R}^n$, we use PSNR as our evaluation metric, where higher PSNR corresponds to smaller $\mathbb{E}[\|X_t - X_T\|^2]$.

With fixed $\gamma_k = 0.001$ and $N = 100$, we first verify that $K \in \{40, 60, 80\}$ yields nearly identical PSNR (mean difference $< 0.1\text{dB}$), suggesting K has minimal impact in this experiment. We therefore fix $K = 80$, gradient step size $\gamma_k = 0.001$, total iteration number $N = 100$, and then evaluate the impact of varying h_k on the deblurring task. fig. 2 presents the PSNR curve after K -th iteration for different h_k configurations (final PSNR = $\{33.23, 33.55, 33.95\}$ for $h_k = \{0, 0.3, 0.7\}$). The results show that an appropriately chosen h_k ensures higher PSNR with fewer iteration numbers, implying smaller $\|X_t - X_T\|^2$ —consistent with our theoretical results in proposition 5.3.1 and theorem 5.3.3. However, excessively large h_k values degrade performance due to poor sequence convergence.

Schedule of $1 - l_k$: With all other settings fixed, we set gradient step size $\gamma_k = 0.001$, total iteration number $N = 100$, $h_k = 0$, and then evaluate the impact of $1 - l_k$ on the deblurring task using the CelebA dataset. table 3 presents the final PSNR and SSIM values for different λ


 FIGURE 2. Study on h_k

Schedule	PSNR	SSIM
[29]	32.23	0.9361
$\lambda = 0.90$	28.99	0.7237
$\lambda = 0.94$	32.92	0.8837
$\lambda = 0.96$	34.49	0.9479
$\lambda = 0.99$	30.36	0.8984

 TABLE 3. Study on $1-l_k$

	PSNR	SSIM
With L_u	33.53	0.9401
W/o L_u	33.14	0.9358

TABLE 4. Study on Lipschitz Penalty

configurations. The second row in table 3 uses the schedule proposed in PnP-Flow, the 3-6 rows use our proposed schedule eq. (23) with four different λ . As discussed in section 5.1, a proper λ can significantly improve the generated image quality in terms of PSNR and SSIM.

Lipschitz Penalty L_u : With all other settings fixed, we set step size $\gamma_k = 0.001$, total iteration number $N = 100$, $h_k = 0$. We empirically set the coefficient of the Lipschitz penalty loss to be 0.1 and compare our method with and without Lipschitz regularization. Table 4 shows that penalizing the Lipschitz constant improves PSNR and SSIM, aligning with the error analysis in Section 4.

7. CONCLUSION

In this paper, we advance the theoretical and practical understandings of PnP-Flow for image restoration from a continuous-time SDE perspective. Our approach uniquely integrates SDE analysis with discrete PnP-Flow, providing both theoretical rigor and practical improvements for PnP-Flow. As a limitation of our work, we focus on straight-line flows in this paper, generalizing our work to manifold-based flows remains future work. Although developed for PnP-Flow, our methodology can be extended to other generative models and deep learning frameworks. Key future directions include: 1) Extending the SDE analysis to manifold-based flow matching models to broaden applicability. 2) Developing advanced projection techniques for the interpolation step to improve denoising performance. 3) Investigating additional SDE-informed strategies, such as adaptive noise schedules or alternative extrapolation methods, to further enhance efficiency and accuracy. By pursuing these avenues, we aim to further develop the SDE-informed frameworks, making them more robust and versatile tools for image restoration and beyond.

Societal Impacts: Our paper presents an SDE framework for analyzing and improving PnP-Flow. Imaging is a fundamental technique for many of the modern scientific disciplines, improving imaging algorithms will have foundational impact on these disciplines. We do not see additional negative societal impact compared to existing approaches due to our work.

APPENDIX A. ADDITIONAL EXPERIMENTAL DETAILS

A.1. Frobenius Norm Estimator. For a $n \times n$ matrix \mathbf{A} , its trace can be unbiasedly estimated by [18]

$$(44) \quad \text{Trace}(\mathbf{A}) = \mathbb{E}_{\epsilon \sim p(\epsilon)} [\epsilon^\top \mathbf{A} \epsilon]$$

, where $p(\epsilon)$ is a n -dimensional distribution s.t. $\mathbb{E}[\epsilon] = \mathbf{0}$ and $\text{Cov}[\epsilon] = \mathbf{I}_{n \times n}$ and $p(\epsilon)$ is always chosen as standard Gaussian. Then given a vector field regressor $\tilde{\epsilon}(t, X_t)$, the Frobenius norm of the

Jacobian can be estimated

$$\begin{aligned}
 \|\nabla_{\mathbf{x}} \tilde{\mathbf{u}}_t(X_t)\|_F^2 &= \text{Trace}(\nabla_{\mathbf{x}} \tilde{\mathbf{u}}_t(X_t)^\top \nabla_{\mathbf{x}} \tilde{\mathbf{u}}_t(X_t)) \\
 (45) \quad &= \mathbb{E}_{\epsilon \sim p(\epsilon)} [\epsilon^\top \nabla_{\mathbf{x}} \tilde{\mathbf{u}}_t(X_t)^\top \nabla_{\mathbf{x}} \tilde{\mathbf{u}}_t(X_t) \epsilon] \\
 &= \mathbb{E}_{\epsilon \sim p(\epsilon)} [\|\nabla_{\mathbf{x}} \tilde{\mathbf{u}}_t(X_t) \epsilon\|_2^2]
 \end{aligned}$$

and notice the fact that $\|\nabla_{\mathbf{x}} \tilde{\mathbf{u}}_t(X_t)\|_2 \leq \|\nabla_{\mathbf{x}} \tilde{\mathbf{u}}_t(X_t)\|_F$ and $L_u = \sup_{X \in \mathbb{R}^n} \|\nabla_{\mathbf{x}} \tilde{\mathbf{u}}_t(X_t)\|_2$. So penalizing Eq.(45) serves to constrain the Lipschitz constant.

Given the influence of the Lipschitz constant L_u of the estimated vector field $\tilde{\mathbf{u}}$ (or $\tilde{\mathbf{u}}$) on error bounds and convergence rates, we introduce an FM model regularized by a Lipschitz penalty term (see section 4.1). We use the same training settings in [29]. We use the pre-trained model provided by [29] as the baseline model.

A.2. Hyper-parameter Setting. We list the hyper-parameters used for our method on the CelebA dataset and AFHQ-Cat dataset in the following two tables.

TABLE 5. Hyper-parameters used for our method on the CelebA dataset.

	Denoising	Deblurring	Super-resolution	Random Inpainting	Box Inpainting
r_k (gradient step size)	0.004	0.003	0.002	0.0002	0.0012
h_k (extrapolation step size)	0.5	0.5	0.5	0.5	0.5
$\lambda (1 - l_k)$	0.965	0.965	0.965	0.965	0.965
N (number of iterations)	100	100	100	100	100
K (SDE t_0)	80	80	80	80	80

TABLE 6. Hyper-parameters used for our method on the AFHQ-Cat dataset.

	Denoising	Deblurring	Super-resolution	Random Inpainting	Box Inpainting
r_k (gradient step size)	0.004	0.0045	0.004	0.0002	0.002
h_k (extrapolation step size)	0.3	0.3	0.3	0.3	0.3
$\lambda (1 - l_k)$	0.965	0.965	0.965	0.965	0.965
N (number of iterations)	100	100	100	100	100
K (SDE t_0)	80	80	80	80	80

A.3. Additional Visual Results. In this section, we provide some additional visual results for comparison.

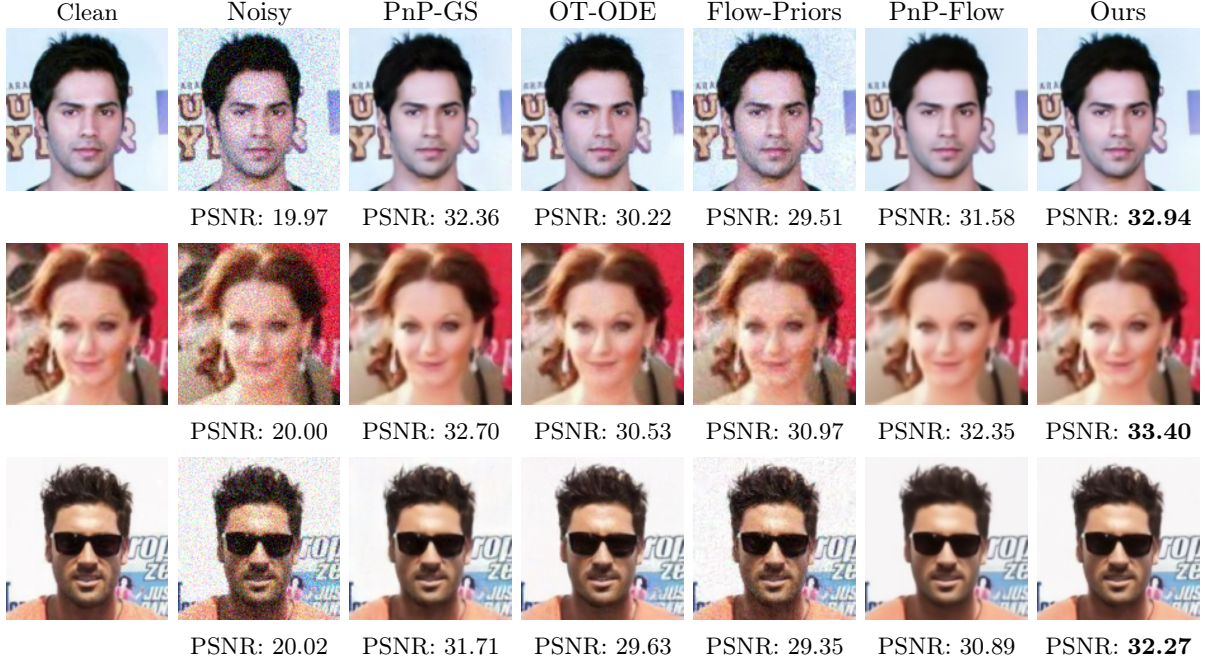


FIGURE 3. Comparison of image denoising results on CelebA.

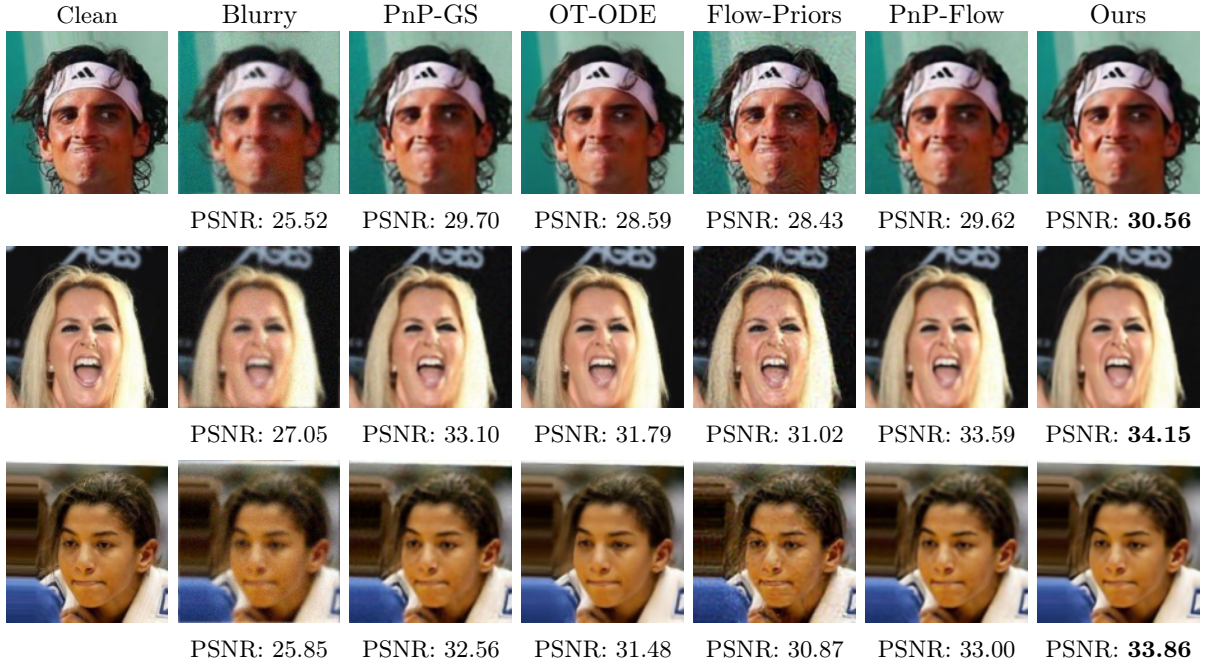


FIGURE 4. Comparison of image deblurring results on CelebA.

ACKNOWLEDGMENTS

We would like to acknowledge the assistance of volunteers in putting together this example manuscript and supplement.

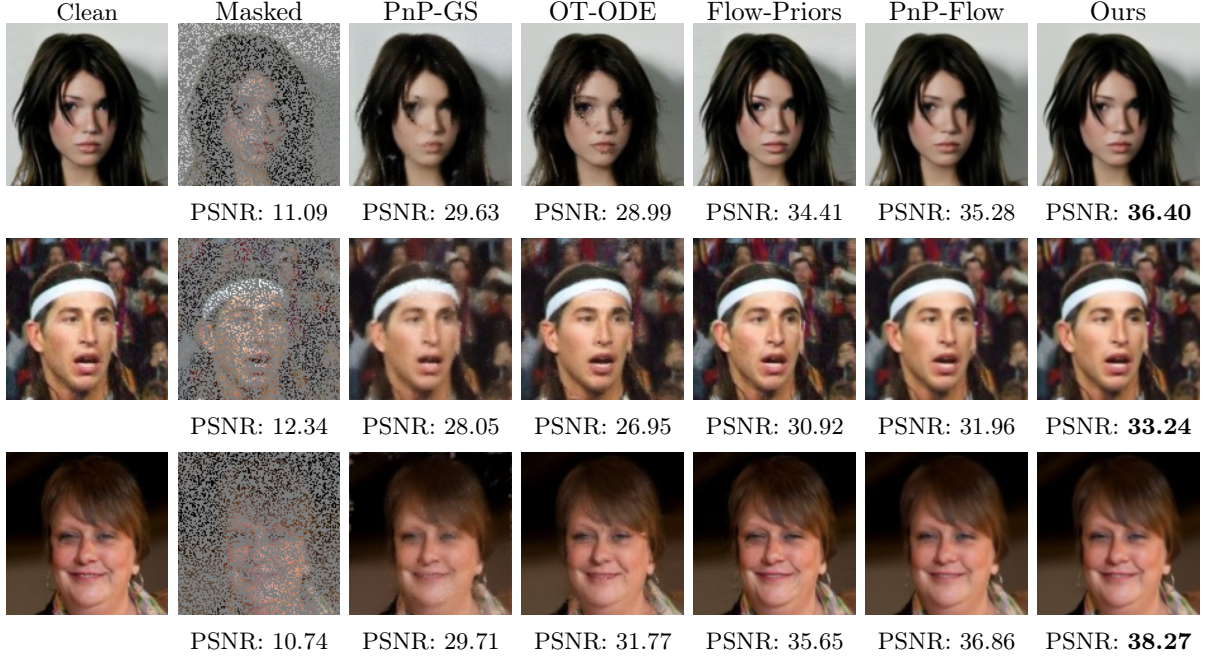


FIGURE 5. Comparison of random inpainting results on CelebA.

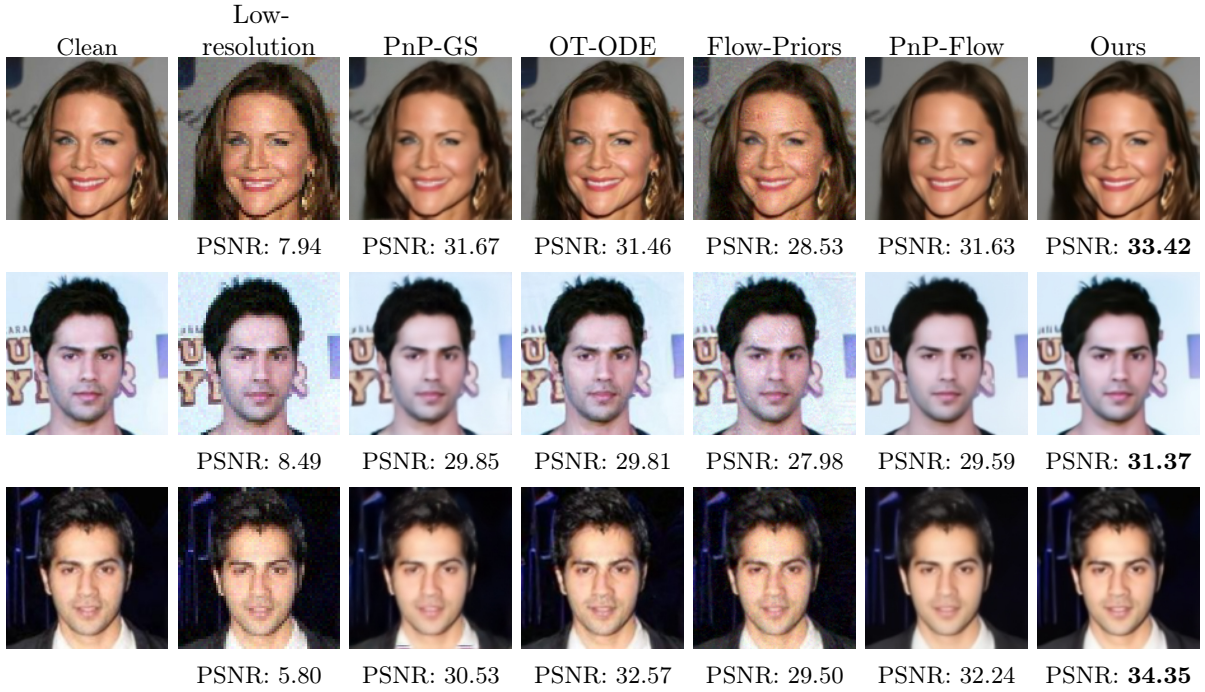


FIGURE 6. Comparison of super-resolution results on CelebA.

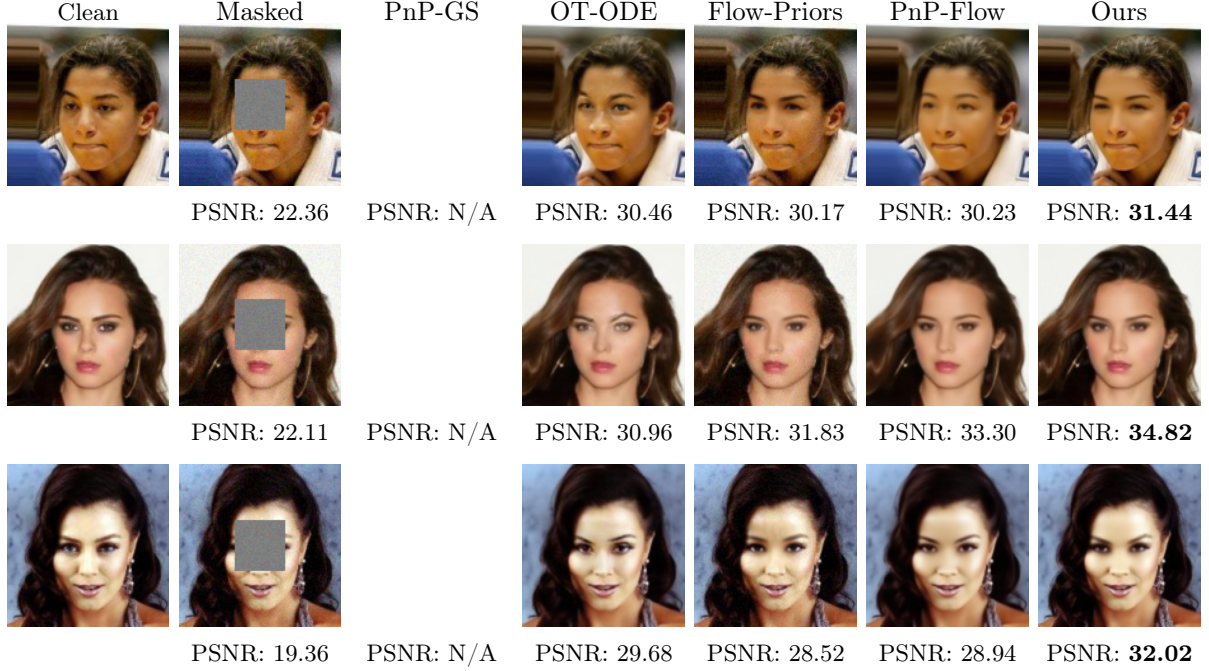


FIGURE 7. Comparison of box inpainting results on CelebA.



FIGURE 8. Comparison of image denoising results on AFHQ-Cat.

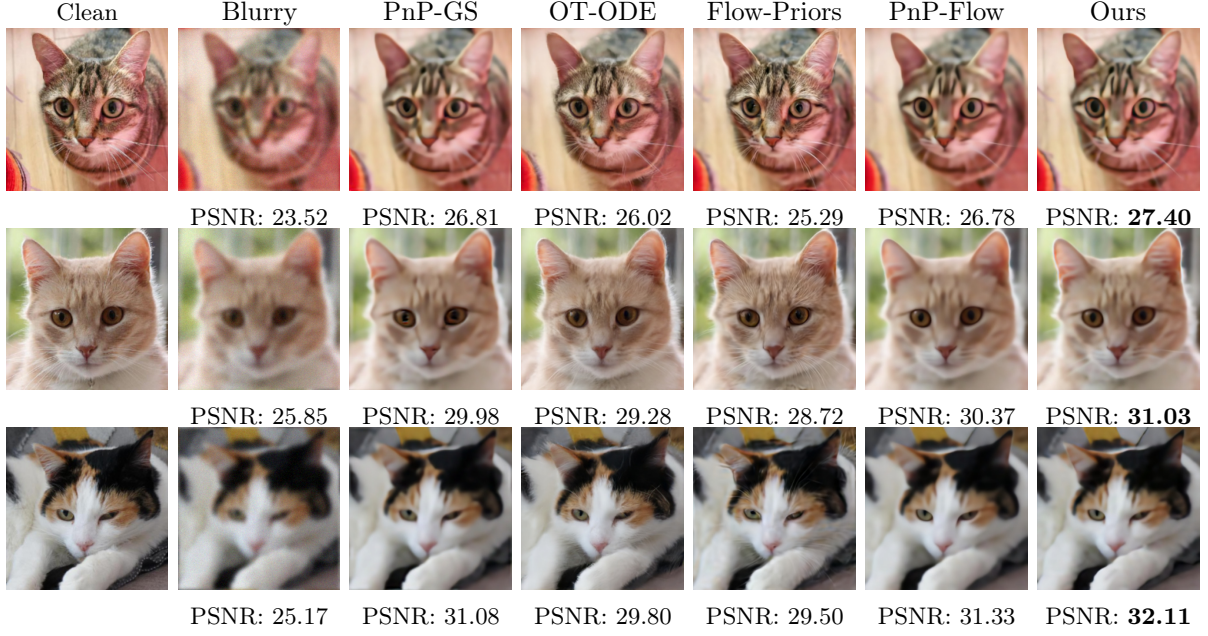


FIGURE 9. Comparison of image deblurring results on AFHQ-Cat.

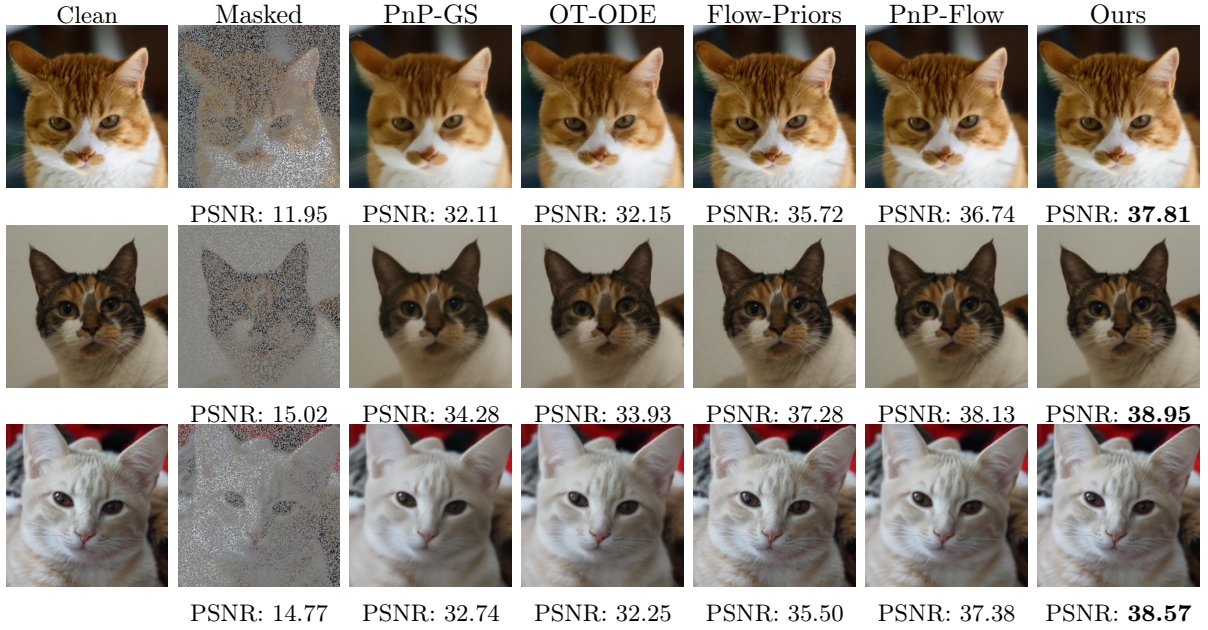


FIGURE 10. Comparison of random inpainting results on AFHQ-Cat.

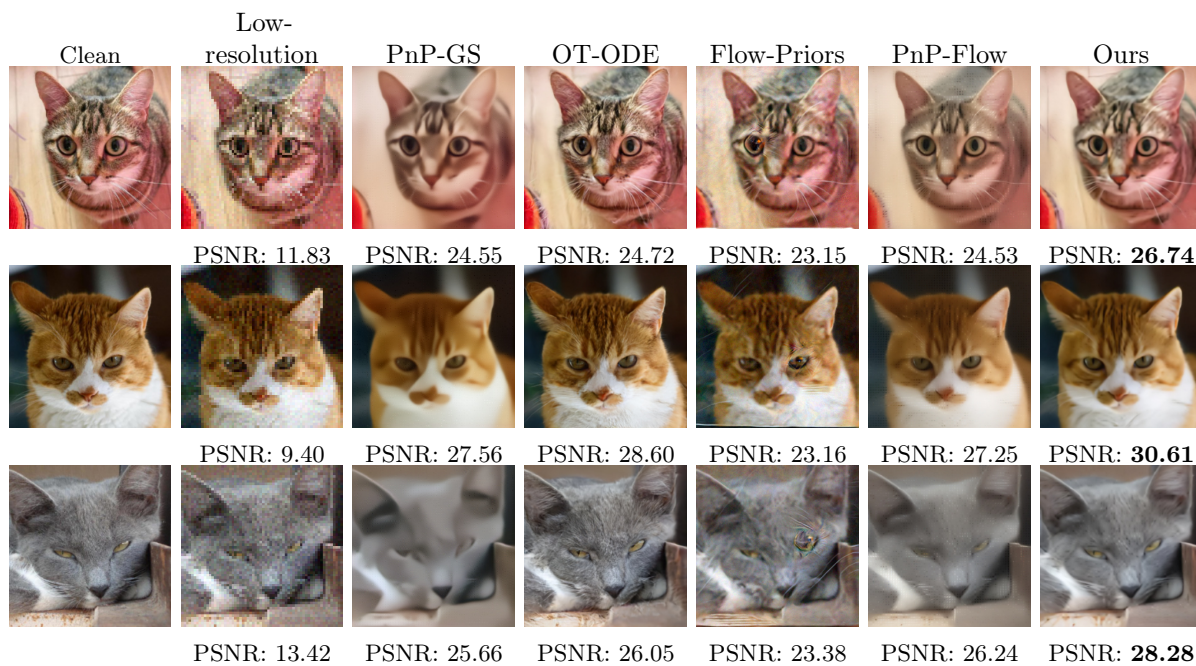


FIGURE 11. Comparison of super-resolution results on AFHQ-Cat.

REFERENCES

1. Michael Samuel Albergo and Eric Vanden-Eijnden, *Building normalizing flows with stochastic interpolants*, The Eleventh International Conference on Learning Representations, 2023.
2. Martin Arjovsky, Soumith Chintala, and Léon Bottou, *Wasserstein generative adversarial networks*, International conference on machine learning, PMLR, 2017, pp. 214–223.
3. Amir Bar, Yossi Gandelsman, Trevor Darrell, Amir Globerson, and Alexei Efros, *Visual prompting via image inpainting*, Advances in Neural Information Processing Systems **35** (2022), 25005–25017.
4. Heli Ben-Hamu, Omri Puny, Itai Gat, Brian Karrer, Uriel Singer, and Yaron Lipman, *D-flow: Differentiating through flows for controlled generation*, arXiv preprint arXiv:2402.14017 (2024).
5. Ashish Bora, Ajil Jalal, Eric Price, and Alexandros G Dimakis, *Compressed sensing using generative models*, International Conference on Machine Learning (ICML), PMLR, 2017, pp. 537–546.
6. Antoni Buades, Bartomeu Coll, and Jean-Michel Morel, *A review of image denoising algorithms, with a new one*, Multiscale modeling & simulation **4** (2005), no. 2, 490–530.
7. Sitan Chen, Sinho Chewi, Holden Lee, Yuanzhi Li, Jianfeng Lu, and Adil Salim, *The probability flow ode is provably fast*, Advances in Neural Information Processing Systems **36** (2023), 68552–68575.
8. Yunjey Choi, Youngjung Uh, Jaejun Yoo, and Jung-Woo Ha, *Stargan v2: Diverse image synthesis for multiple domains*, Proceedings of the IEEE/CVF conference on computer vision and pattern recognition, 2020, pp. 8188–8197.
9. Hyungjin Chung, JaeHyun Kim, and Jong Chul Lee, *Diffusion posterior sampling for general noisy inverse problems*, International Journal of Computer Vision (IJCV) **131** (2023), 1180–1196.
10. Hyungjin Chung, Chitwan Saharia, William Chan, Tim Salimans, Jonathan Ho, Jong Chul Lee, and Ben Poole, *Come-closer-diffuse-faster: Accelerating conditional diffusion models for inverse problems through stochastic localization*, Advances in Neural Information Processing Systems (NeurIPS), vol. 35, 2022, pp. 26184–26197.
11. Regev Cohen, Michael Elad, and Peyman Milanfar, *Regularization by denoising via fixed-point projection (red-pro)*, SIAM Journal on Imaging Sciences **14** (2021), no. 3, 1374–1406.
12. Michael Elad, Bahjat Kawar, and Gregory Vaksman, *Image denoising: The deep learning revolution and beyond—a survey paper*, SIAM Journal on Imaging Sciences **16** (2023), no. 3, 1594–1654.
13. Yuchen Fan, Jiahui Yu, Yiqun Mei, Yulun Zhang, Yun Fu, Ding Liu, and Thomas S Huang, *Neural sparse representation for image restoration*, Advances in Neural Information Processing Systems **33** (2020), 15394–15404.
14. Ishaan Gulrajani, Faruk Ahmed, Martin Arjovsky, Vincent Dumoulin, and Aaron C Courville, *Improved training of wasserstein gans*, Advances in neural information processing systems **30** (2017).
15. Yan Huang, Shang Li, Liang Wang, Tieniu Tan, et al., *Unfolding the alternating optimization for blind super resolution*, Advances in Neural Information Processing Systems **33** (2020), 5632–5643.
16. Yuhao Huang, Qingsong Wang, Akwum Onwunta, and Bao Wang, *Efficient score matching with deep equilibrium layers*, The Twelfth International Conference on Learning Representations, 2024.
17. Samuel Hurault, Arthur Leclaire, and Nicolas Papadakis, *Gradient step denoiser for convergent plug-and-play*, arXiv preprint arXiv:2110.03220 (2021).
18. Michael F Hutchinson, *A stochastic estimator of the trace of the influence matrix for laplacian smoothing splines*, Communications in Statistics-Simulation and Computation **18** (1989), no. 3, 1059–1076.
19. Franck Iutzeler and Jérôme Malick, *On the proximal gradient algorithm with alternated inertia*, Journal of Optimization Theory and Applications **176** (2018), no. 3, 688–710.
20. Fan Jia, Shen Mao, Xue-Cheng Tai, and Tieyong Zeng, *A variational model for nonuniform low-light image enhancement*, SIAM Journal on Imaging Sciences **17** (2024), no. 1, 1–30.
21. Fan Jia, Wing Hong Wong, and Tieyong Zeng, *Ddunet: Dense dense u-net with applications in image denoising*, Proceedings of the IEEE/CVF international conference on computer vision, 2021, pp. 354–364.
22. Mostafa Kadkhodaie and Eero P Simoncelli, *Stochastic denoising score matching: A unifying framework for learning deep generative models*, Advances in Neural Information Processing Systems (NeurIPS), vol. 34, 2021, pp. 12430–12443.
23. Bahjat Kawar, Michael Elad, Stefano Ermon, and Jiaming Song, *Denoising diffusion restoration models*, Advances in Neural Information Processing Systems **35** (2022), 23593–23606.
24. Peter E Kloeden, Eckhard Platen, Peter E Kloeden, and Eckhard Platen, *Stochastic differential equations*, Springer, 1992.
25. Yaron Lipman, Ricky TQ Chen, Heli Ben-Hamu, Maximilian Nickel, and Matt Le, *Flow matching for generative modeling*, arXiv preprint arXiv:2210.02747 (2022).
26. Xingchao Liu, Chengyue Gong, and qiang liu, *Flow straight and fast: Learning to generate and transfer data with rectified flow*, The Eleventh International Conference on Learning Representations, 2023.

27. Cheng Lu, Kaiwen Zheng, Fan Bao, Jianfei Chen, Chongxuan Li, and Jun Zhu, *Maximum likelihood training for score-based diffusion odes by high order denoising score matching*, International Conference on Machine Learning, PMLR, 2022, pp. 14429–14460.
28. Long Ma, Tengyu Ma, Risheng Liu, Xin Fan, and Zhongxuan Luo, *Toward fast, flexible, and robust low-light image enhancement*, Proceedings of the IEEE/CVF conference on computer vision and pattern recognition, 2022, pp. 5637–5646.
29. Ségolène Tiffany Martin, Anne Gagneux, Paul Hagemann, and Gabriele Steidl, *Pnp-flow: Plug-and-play image restoration with flow matching*, The Thirteenth International Conference on Learning Representations, 2025.
30. Takeru Miyato, Toshiaki Kataoka, Masanori Koyama, and Yuichi Yoshida, *Spectral normalization for generative adversarial networks*, arXiv preprint arXiv:1802.05957 (2018).
31. Bernt Oksendal, *Stochastic differential equations: an introduction with applications*, Springer Science & Business Media, 2013.
32. Naama Pearl, Tali Treibitz, and Simon Korman, *Nan: Noise-aware nerfs for burst-denoising*, Proceedings of the IEEE/CVF Conference on Computer Vision and Pattern Recognition, 2022, pp. 12672–12681.
33. Thomas Pock and Shoham Sabach, *Inertial proximal alternating linearized minimization (ipalm) for nonconvex and nonsmooth problems*, SIAM journal on imaging sciences **9** (2016), no. 4, 1756–1787.
34. Ashwini Pokle, Matthew J Muckley, Ricky TQ Chen, and Brian Karrer, *Training-free linear image inverses via flows*, arXiv preprint arXiv:2310.04432 (2023).
35. Yuhui Quan, Zicong Wu, and Hui Ji, *Gaussian kernel mixture network for single image defocus deblurring*, Advances in Neural Information Processing Systems **34** (2021), 20812–20824.
36. Ernest Ryu, Jialin Liu, Sicheng Wang, Xiaohan Chen, Zhangyang Wang, and Wotao Yin, *Plug-and-play methods provably converge with properly trained denoisers*, International Conference on Machine Learning, PMLR, 2019, pp. 5546–5557.
37. Viral Shah, Seyed Kamyar Seyed Ghasemipour, Ioannis Mitliagkas, Aditi Raghunathan Goyal, and Satyen Kale, *Solving linear inverse problems using gans*, International Conference on Machine Learning (ICML) Workshop on Implicit Models, 2018.
38. Jiaming Song, Qingsheng Zhang, Hongxu Yin, Morteza Mardani, Ming-Yu Liu, Jan Kautz, Yongxin Chen, and Arash Vahdat, *Loss-guided diffusion models for plug-and-play controllable generation*, International Conference on Machine Learning, PMLR, 2023, pp. 32483–32498.
39. Weijie Su, Stephen Boyd, and Emmanuel J Candes, *A differential equation for modeling nesterov’s accelerated gradient method: Theory and insights*, Journal of Machine Learning Research **17** (2016), no. 153, 1–43.
40. Hong Ye Tan, Subhadip Mukherjee, Junqi Tang, and Carola-Bibiane Schönlieb, *Provably convergent plug-and-play quasi-newton methods*, SIAM Journal on Imaging Sciences **17** (2024), no. 2, 785–819.
41. Singanallur V Venkatakrishnan, Charles A Bouman, and Brendt Wohlberg, *Plug-and-play priors for model based reconstruction*, 2013 IEEE global conference on signal and information processing, IEEE, 2013, pp. 945–948.
42. Zhongming Wu, Chaoyan Huang, and Tieyong Zeng, *Extrapolated plug-and-play three-operator splitting methods for nonconvex optimization with applications to image restoration*, SIAM Journal on Imaging Sciences **17** (2024), no. 2, 1145–1181.
43. Zihui Wu, Yu Sun, Yifan Chen, Bingliang Zhang, Yisong Yue, and Katherine Bouman, *Principled probabilistic imaging using diffusion models as plug-and-play priors*, Advances in Neural Information Processing Systems **37** (2024), 118389–118427.
44. Xiaogang Xu, Ruixing Wang, Chi-Wing Fu, and Jiaya Jia, *Snr-aware low-light image enhancement*, Proceedings of the IEEE/CVF conference on computer vision and pattern recognition, 2022, pp. 17714–17724.
45. Xingyu Xu and Yuejie Chi, *Provably robust score-based diffusion posterior sampling for plug-and-play image reconstruction*, arXiv preprint arXiv:2403.17042 (2024).
46. Yangyang Xu and Wotao Yin, *A block coordinate descent method for regularized multiconvex optimization with applications to nonnegative tensor factorization and completion*, SIAM Journal on imaging sciences **6** (2013), no. 3, 1758–1789.
47. Shuo Yang, Ping Luo, Chen-Change Loy, and Xiaoou Tang, *From facial parts responses to face detection: A deep learning approach*, Proceedings of the IEEE international conference on computer vision, 2015, pp. 3676–3684.
48. Raymond A Yeh, Chen Chen, Teck Yian Lim, Alexander G Schwing, Mark Hasegawa-Johnson, and Minh N Do, *Semantic image inpainting with deep generative models*, Proceedings of the IEEE conference on computer vision and pattern recognition, 2017, pp. 5485–5493.
49. Kaihao Zhang, Wenhan Luo, Yiran Zhong, Lin Ma, Bjorn Stenger, Wei Liu, and Hongdong Li, *Deblurring by realistic blurring*, Proceedings of the IEEE/CVF conference on computer vision and pattern recognition, 2020, pp. 2737–2746.
50. Kaihao Zhang, Wenqi Ren, Wenhan Luo, Wei-Sheng Lai, Björn Stenger, Ming-Hsuan Yang, and Hongdong Li, *Deep image deblurring: A survey*, International Journal of Computer Vision **130** (2022), no. 9, 2103–2130.

51. Yasi Zhang, Peiyu Yu, Yaxuan Zhu, Yingshan Chang, Feng Gao, Ying Nian Wu, and Oscar Leong, *Flow priors for linear inverse problems via iterative corrupted trajectory matching*, arXiv preprint arXiv:2405.18816 (2024).
52. Yuanzhi Zhu, Kai Zhang, Jingyun Liang, Jiezhong Cao, Bihan Wen, Radu Timofte, and Luc Van Gool, *Denoising diffusion models for plug-and-play image restoration*, Proceedings of the IEEE/CVF Conference on Computer Vision and Pattern Recognition, 2023, pp. 1219–1229.

(Fan Jia, Yuhao Huang, Shih-Hsin Wang, Bao Wang) DEPARTMENT OF MATHEMATICS, UNIVERSITY OF UTAH, SALT LAKE CITY, UT 84112, USA

Email address, Fan Jia: `fan.jia@utah.edu`

Email address, Yuhao Huang: `u1430219@utah.edu`

Email address, Shih-Hsin Wang: `u1371684@utah.edu`

Email address, Bao Wang: `bwang@math.utah.edu`

(Cristina Garcia-Cardona) LOS ALAMOS NATIONAL LABORATORY, LOS ALAMOS, USA

Email address, Cristina Garcia-Cardona: `cgarcia@lanl.gov`

(Andrea L. Bertozzi) DEPARTMENT OF MATHEMATICS, UNIVERSITY OF CALIFORNIA, LOS ANGELES, USA

Email address, Andrea L. Bertozzi: `bertozzi@math.ucla.edu`